Université du Québec
à Rimouski

MODELISATION DE L'EFFET DES HYDROCARBURES SUR LE SYSTEME PLANCTONIQUE DU GOLFE SAN JORGE, ARGENTINE

MÉMOIRE PRÉSENTÉ

dans le cadre du programme de maîtrise en océanographie

en vue de l'obtention du grade de maître ès sciences

PAR

©PHILIPPE KLOTZ

Août 2018

Composition du jury :

Cédric Chavanne, président du jury, Université du Québec à Rimouski

Irene Schloss, directrice de recherche, Instituto Antártico Argentino et Centro Austral de Investigaciones Científicas (CADIC-CONICET)

Dany Dumont, codirecteur de recherche, Université du Québec à Rimouski

Diane Lavoie, examinatrice externe, Institut Maurice Lamontagne

Dépôt final le 31 Août 2018

REMERCIEMENTS

Ce projet prend sa place dans une large collaboration entre l'Argentine et le Canada et n'aurait pu voir le jour sans la participation de nombreux acteurs. Tout d'abord, nous aimerions remercier le Conseil de Recherches en Sciences Naturelles et en Génie (CRSNG) pour leur contribution financière. Dans le cadre de la diffusion de notre projet à l'échelle nationale et internationale, nous remercions Québec Océan et l'Université du Québec à Rimouski (UQAR) pour leur précieuse aide. Nous remercions sincèrement la contribution du Ministerio de Ciencia, Tecnología e Innovación Productiva (MINCyT), de la Province de Chubut ainsi que du Consejo Nacional de Investigaciones Científicas y Técnicas (CONICET) en Argentine.

Personnellement, mes remerciements iront d'abord aux participants de la mission PROMESse avec qui j'ai partagé la houle, les paysages et éventuellement quelques mots d'espagnol : l'équipage du Coriolis II, Guillermo, Cédric, Valérie , Gesche, Sylvain, Gilles, Aline, notre cher Gus et les nombreuses personnes que j'oublie. Ensuite, j'aimerais remercier tous les étudiants de ma promotion de maîtrise en océanographie pour tous les échanges que nous avons eu qui m'ont fait réfléchir et remettre en question ma façon de penser jusqu'à présent. A ceux-là s'ajoute une liste exhaustive de personnes présentes à l'ISMER qui ont contribué de proche ou de loin à mon évolution au Québec : Paul, Mélanie, Pierre-Arnaud, Pascal, Robin, Julien, Marion et bien d'autres. J'aimerais à présent remercier mes merveilleux et irremplaçables directeurs de maîtrise qui m'ont avant tout fait confiance et soutenu malgré mes nombreuses difficultés à apprendre ce que représente une facette de la modélisation numérique. Enfin, je dois ma place au Québec en grande partie à mes parents, mes soeurs et mon parrain qui m'ont soutenu moralement et financièrement afin de réaliser mes objectifs de vie. Mille merci.

RÉSUMÉ

L'écosystème côtier du golfe San Jorge (GSJ), situé à l'est du plateau de Patagonie (Argentine) est reconnu pour son importante productivité biologique permettant d'y soutenir la pêche industrielle et certaines activités touristiques. Depuis le début du XX^{ème}, l'exploitation d'importants gisements pétroliers terrestres dans les provinces de Chubut et Santa-Cruz représente la moitié de la production d'hydrocarbures pétrolifères du pays. Dans l'avenir, cette exploitation pourrait s'étendre à l'environnement marin et par conséquent, menacer son équilibre actuel. Cette étude numérique, réalisée en parallèle de la mission PROMESse 2014, vise à comprendre la réponse de la dynamique planctonique dans la zone sud-est du GSJ lors d'une contamination chronique éventuelle par des hydrocarbures (HC). Nous présentons ici un modèle biogéochimique à onze compartiments couplé à un modèle de turbulence dans lequel nous avons paramétrisé les processus biologiques liés à la contamination, tels que la biodégradation des HC, la croissance et la mortalité du zoo- et du bactérioplancton. Un scénario de contamination chronique en surface, incluant plusieurs niveaux de perturbation, est appliqué à deux environnements physiquement contrastés retrouvé de part et d'autre d'un front d'origine tidale, une colonne d'eau bien mélangée et une colonne d'eau stratifiée. Les résultats de ces simulations montrent que, pour chaque niveau de perturbation, la biodégradation ne débute qu'au début de l'été avec l'augmentation de la biomasse bactérioplanctonique, lorsque la production primaire augmente. Le phytoplancton, notamment les diatomées, présentent une croissance élevée plus le niveau de perturbation est élevé. Cette tendance peut être associée à la diminution importante de la concentration zooplanctonique subissant la toxicité des HC dans la zone euphotique, limitant ainsi le broutage. De manière indirecte, l'ajout d'HC dans le système entraine aussi une augmentation de la production de détritus, résultant de l'augmentation de la mortalité du zooplancton mais aussi de l'augmentation des biomasses bactérienne et phytoplanctonique. Alors que les effets des HC semblent être plus marqués dans l'environnement stratifié, l'environnement bien-mélangé présente des concentrations en HC plus faibles et limite donc les effets directs et indirects sur les compartiments zoo- et phytoplanctonique.

Mots clés : modélisation, cycles biogéochimiques, turbulence, hydrocarbures, écotoxicité, plancton, biodégradation

ABSTRACT

The coastal ecosystem of the San Jorge Gulf (SJG), located on the east part the Patagonian shelf (Argentina), is known for its high biological productivity supporting industrial fishing and some tourism activities. Since the beginning of the 20^{th} century, the exploitation of large oil fields in the provinces of Chubut and Santa Cruz has contributed to half of the country's hydrocarbon petroleum production. In the future, this exploitation could be extended to the marine environment, consequently threatening its current state. This numerical study, carried out in parallel with the PROMESse 2014 mission, aims at understanding the planktonic dynamics in the south-eastern SJG zone during a potential chronic contamination by hydrocarbons (HC). We present here an eleven-compartment biogeochemical model coupled with a turbulence model in which we have parameterized biological processes related to contamination, such as biodegradation, growth and mortality of zoo- and bacterioplankton. A chronic surface contamination scenario, including several levels of disturbance, is applied to two physically contrasting environments found on either side of a tidally induced frontal zone, a well-mixed water column, and a stratified water column. The results of these simulations show that, for each level of disturbance, biodegradation only begins at the beginning of summer with the increase of bacterioplankton biomass, when the primary production increases. Phytoplankton, especially diatoms, shows high growth rates the higher the level of disturbance. This trend may be associated with the significant decrease in zooplankton concentration undergoing HC toxicity in the euphotic zone, thus limiting grazing. Indirectly, the addition of HC in the system also results in an increase of detritus production, resulting from increased zooplankton mortality but also from increased bacterial and phytoplanktonic biomasses. While the effects of HC seem to be more pronounced in the stratified environment, the well-mixed environment shows lower, more diluted concentrations of HC and therefore limits the direct and indirect effects on zoo- and phytoplankton compartments.

Keywords : modelling, biogeochemical cycles, turbulence, hydrocarbons, ecotoxicity, plankton, biodegradation

TABLE DES MATIÈRES

LISTE DES TABLEAUX

LISTE DES FIGURES

LISTE DES ABRÉVIATIONS

EAI	Eaux Antarctiques Intermédiaires
GOTM	General Ocean Turbulence Model
GSJ	Golfe San Jorge
HAP	Hydrocarbure Aromatique Polycyclique
HC	Hydrocarbure / Hydrocarbon
LDON	Labile Dissolved Organic Nitrogen
LME	Large Marine Ecosystem
OHCB	Obligate Hydrocarbon-Degrading Bacteria
PAH	Polycyclic Aromatic Hydrocarbon
PROMESse	Programme multidisciplinaire de recherche en océanographie pour l'étude de l'écosystème du golfe San Jorge et de la côte de la province de Chubut
SJG	San Jorge Gulf
SWAS	Southwestern Atlantic Shelf
SST	Sea Surface Temperature
CST	Complete version of the model simulated for the STratified experiment
CWM	Complete version of the model simulated for the Well-Mixed experiment

INTRODUCTION GÉNÉRALE

Contexte et problématique

Le plateau de Patagonie en Argentine, situé dans l'Océan Atlantique Sud-Ouest est considéré comme l'un des écosystèmes les plus productifs de la planète (Bisbal, 1995; Guerrero et al., 1999; Acha et al., 2004). La production primaire abondante permet d'y soutenir de manière importante l'activité de pêche industrielle depuis la fin des années 1970 (Csirke, 1987). Dans cette région, en particulier dans le golfe de San Jorge (GSJ), l'exploitation terrestre du pétrole est depuis le début du XX^{e} siècle, la principale ressource économique de la région représentant aujourd'hui la moitié de la production argentine (Ministerio de Energía y Minería, 2016). Le développement successif de villes portuaires telles que Comodoro Rivadavia et Caleta Olivia a permis la valorisation des ressources naturelles du golfe comme la pêche et le tourisme.

Le pétrole brut, acheminé par voies maritimes à partir des ports ci-dessus vers des centres de raffineries comme celui de La Plata, pourrait déjà contribuer à une contamination chronique de l'écosystème cotier. Cependant, aucune étude d'impact n'a été réalisée jusqu'à présent. De surcroît, le gouvernement argentin envisage la prospection de nouveaux gisements au sein du milieu marin. L'exploration et l'extraction de ces ressources pétrolifères représentent un risque pour l'écosystème et ses ressources naturelles. Toutefois, l'impact d'une pollution éventuelle sur la pêche, pour être évaluée adéquatement, requiert une connaissance des interactions écologiques associées à une telle pollution, ce qui fait défaut actuellement, comme nous le verrons plus bas. Il est donc essentiel d'acquérir plus de connaissances de base sur la dynamique physique et biogéochimique de l'écosytème du GSJ avant les activités d'exploitation.

Le plateau peut être divisé en trois grandes zones distinctes : la région du courant des Malouines, les eaux du plateau subantarctique et le système côtier (Carreto et al., 1995). À la rupture du plateau, la remontée d'eaux profondes associée au courant des Malouines engendre la formation de fronts de méso-échelle (Piola and Rivas, 1997). Ces eaux riches en nutriments, advectées jusqu'à la zone euphotique, favorisent ainsi le développement du phytoplancton (Carreto et al., 1995; Rivas et al., 2006). Sur le plateau, la formation de plusieurs fronts de sous méso-échelle d'origine tidale est corrélée à l'appartition de zones de forte production. Des mesures *in situ* de chlorophylle-*a* ainsi que des données satellitaires confirment leur apparition durant le printemps et l'été austral (Akselman and Carreto, 1996; Rivas et al., 2006; Carreto et al., 2007).

Localisé entre les latitudes 45° et 47° S, dans la bande des quarantièmes rugissants, le GSJ est exposé aux vents d'ouest soutenus tout au long de l'année. Ceux-ci, ainsi que de fortes amplitudes de marées, induites par les constantes semi-diurnes M_2 and S_2 dominantes, contribuent à une circulation antihoraire des masses d'eau (Glorioso and Simpson, 1994; Palma et al., 2004). Le GSJ est caractérisé par des profondeurs dépassant rarement les 100 m sans aucune rupture de pente, cependant, dans la région peu profonde ($\leq$ 80 m) du sud-est du GSJ, une friction importante sur le fond due à l'intensité des courants de marée entraine une forte dissipation de l'énergie tidale et par conséquent un mélange turbulent efficace (Glorioso and Flather, 1995). Ce phénomène permet le maintien d'une zone frontale permanente dans cette région particulière du golfe (Glorioso and Flather, 1997). De plus, les observations satellitaires de température et de concentrations en chlorophylle-*a* y indiquent la présence de gradients horizontaux de surface élevés (Acha et al., 2004; Rivas et al., 2006). Les résultats de simulations numériques de la circulation du plateau de Patagonie présentent de faibles valeurs du paramètre de Simpson-Hunter ($\log_{10}$ (H / U^3 $m^2 s^{-3}$) $\leq$ 2) démontrant ainsi la présence d'un front généré majoritairement par la marée

(Palma et al., 2004; Simpson et al., 1974).

Plusieurs études de la dynamique physique du plateau de Patagonie intègrent le GSJ (Palma et al., 2004; Rivas et al., 2006), cependant peu de données *in situ* permettent d'appuyer ces résultats (Louge et al., 2004). L'intérêt économique des ressources marines de la région a permis la réalisation de plusieurs travaux de caractérisations des communautés benthiques (Fernandez et al., 2003; Fernández et al., 2005), mais, encore une fois, très peu d'études récentes concernent les réseaux trophiques pélagiques et la dynamique verticale du plancton dans le GSJ (Cucchi-Colleoni and Carreto, 2001).

Plusieurs approches de modélisation permettent de simuler la dynamique biogéochimique des systèmes pélagiques. Depuis les années 1970, le développement de modèles numériques biogéochimiques permettant de simuler les processus associés à la production primaire dans des conditions de plus en plus réalistes a permis de mieux comprendre le fonctionnement de l'écosystème pélagique. Fasham et al. (1990) ont proposé un modèle de la dynamique planctonique dans lequel l'azote, considéré comme l'élément limitant de la production, est échangé entre sept (7) compartiments : nitrate, phytoplancton, zooplancton, détritus, azote organique dissous, bactéries et ammonium. Ce modèle s'est particulièrement imposé parce qu'il est suffisament complexe pour aborder des questions biologiques, mais il est suffisament simple pour en tirer une compréhension de la dynamique des systèmes. Comprendre l'évolution spatiale et temporelle d'un assemblage planctonique dans la colonne d'eau implique une connaissance précise de l'environnement physique étudié. Les zones de forte production sont souvent associées à la rencontre de plusieurs masses d'eau de propriétés différentes où la turbulence joue un rôle non seulement dans la disponibilité des nutriments dans la zone euphotique mais aussi dans la distribution de la biomasse phytoplanctonique. Le General Ocean Turbulence Model (GOTM) développé par Burchard et al. (2006) est un modèle de turbulence vertical (1D) auquel peut être

couplé un modèle biogéochimique comme celui de Fasham et al. (1990). Les simulations prennent en compte l'évolution annuelle de la profondeur de mélange et soulignent l'importance de la boucle microbienne dans le renouvèlement de l'azote disponible pour la production primaire.

De nombreuses études ont permis de simuler le comportement des hydrocarbures dans le milieu marin (Reed et al., 1999). Cependant peu de modèles s'intéressent à leur impact sur la dynamique du système planctonique (Gin et al., 2001; Valentine et al., 2012; González et al., 2013). À la suite d'un déversement de pétrole dans le milieu marin, plusieurs processus physico-chimiques et biologiques se mettent en place. À une échelle journalière, l'évolution de la nappe de pétrole est dominée par les processus d'évaporation et de dissolution. Par la suite, l'émulsification, la sédimentation et la biodégradation persistent durant les semaines et mois qui suivent les déversements. La vitesse de chaque processus est directement dépendante des conditions du milieu environnant mais aussi des propriétés physico-chimiques du pétrole. Les Hydrocarbures Aromatiques Polycycliques (HAP) contribuent jusqu'à 60% de la composition totale d'un pétrole brut (Brown et al., 2011). En raison de leur structure particulière, ces composés restent stables après leur dissolution et leur vitesse de dégradation est inversement proportionnelle à la longueur de leur chaine carbonée (Grimes et al., 2011). La solubilité des hydrocarbures dans l'eau varie selon plusieurs paramètres tels que la salinité, la température et la densité du pétrole étudié (Hamam et al., 1988). Parmi les groupes d'hydrocarbures solubles, les HAP présentent le plus d'effets négatifs sur les organismes marins. En effet, le caractère hydrophobe de ces composés et leur biodisponibilité une fois dissous dans l'eau favorise leur adsorption par les organismes marins augmentant leur mortalité par simple toxicité ou par la diminution de leur activité physiologique (Anderson et al., 1974).

Étudier et quantifier les effets des hydrocarbures sur un assemblage planctonique

est difficilement réalisable *in situ*. Les expériences réalisées dans le cadre de micro- et mésocosmes sont une alternative permettant de mieux cibler les effets directs d'une contamination sur un groupe ou une espèce bien définie selon la concentration et le type d'hydrocarbure. De plus le contrôle des conditions de ces cultures permet de mesurer l'influence de variables environnementales telles que la concentration en éléments nutritifs, la température et l'intensité lumineuse sur la croissance, la mortalité et la répartition des organismes étudiés.

Le phytoplancton est l'ensemble d'organismes présentant le plus de variabilité concernant les effets observés après contamination aux hydrocarbures. D'un point de vue biologique, certains groupes semblent plus affectés que d'autres à concentrations équivalentes. C'est le cas des diatomées qui subissent une forte diminution de leur croissance (Hsiao, 1976; Nayar et al., 2005). Cette particularité est attribuée à la composition siliceuse de leurs thèques qui absorbent et accumulent de manière importante les HAP (Siron et al., 1996; Sargian et al., 2007).

La concentration d'hydrocarbures dissous dans l'eau est très variable d'une étude à l'autre allant de 8,6 mg/L (González et al., 2009) à 1400 mg/L (Dahll et al., 1983) et les effets associés à ces concentrations doivent être comparés avec précaution. Gordon and Prouse (1973) considèrent qu'une concentration de 30 à 50 mg/L serait le seuil auquel toute activité cellulaire serait inhibée. González et al. (2009) observent entre 48 et 72 h post-exposition une forte réduction de l'activité photosynthétique et de la production primaire dès 23 mg/L. Au contraire, certains résultats montrent une stimulation de la croissance phytoplanctonique à de faibles concentrations de portion dissoute d'hydrocarbures (Gordon and Prouse, 1973; Dunstan et al., 1975; Hsiao et al., 1978; González et al., 2013). Les mécanismes en lien avec cette augmentation de l'activité photosynthétique sont mal connus et mènent à plusieurs hypothèses : Baker (1971) suggère qu'un apport en éléments

nutritifs est possible à partir de la dégradation d'autres organismes morts par contamination. Gordon and Prouse (1973) mentionnent que l'éventuelle présence de composés retrouvés dans le pétrole permettrait de réguler la croissance de cellules.

Les communautés zooplanctoniques jouent plusieurs rôles écologiques essentiels, notamment dans la régulation de la production primaire et dans le transfert de carbone vers les niveaux trophiques supérieurs. En présence d'hydrocarbures, tous les grands groupes zooplanctoniques semblent être affectés et différents effets sont observables suivant les espèces et les concentrations utilisées. Almeda et al. (2013) étudient les effets du pétrole brut sur un assemblage dominé par les copépodes et mesurent une mortalité de 96% pour une concentration de 100 μl.L^{-1} de HAP. À partir des résultats expérimentaux, ils proposent un modèle sigmoïde de la mortalité du mésozooplancton relatif à la concentration en HAP dans le milieu et calculent une concentration létale moyenne (LC_{50}) de 31.4 μl.L^{-1} après 16 heures d'incubation. La narcose est un des effets observés dans le cadre d'expériences en laboratoire (Barata et al., 2005). Ce processus physiologique encore mal compris est étudié par Almeda et al. (2013) qui montrent que des faibles concentrations (10 à 20 μl.L^{-1}) diminuent de manière notable le métabolisme et les capacités de déplacement des copépodes jusqu'à entrainer la mort de l'organisme.

La biodégradation est un des processus de désagrégation les plus important agissant lors d'une contamination par les hydrocarbures (Beazley et al., 2012). Plusieurs groupes de microorganismes interviennent dans la transformation du pétrole. Depuis le début du XX^{e} siècle, l'étude de leur génome a permis d'isoler près de 200 genres capables de dégrader les hydrocabures (Prince et al., 2003; Head et al., 2006; Cappello et al., 2007). Dans le milieu marin, le bactérioplancton présente des modifications importantes de la structure de sa communauté ainsi que de sa biomasse à la suite d'une marée noire (Hazen et al., 2010; Dubinsky et al., 2013). Ces bactéries marines, nommées « Obligate Hydrocarbon-Degrading

Bacteria » (OHCB) (Yakimov et al., 2007), omniprésentes à de très faibles concentrations dans la colonne d'eau, sont caractérisées par une grande spécificité de substrat. Le genre Alcanivorax (γ-Protéobacteries), par exemple, présente une capacité de réponse très efficace et un développement particulièrement rapide en présence d'hydrocarbures (Syutsubo et al., 2001; Kasai et al., 2002; Cappello et al., 2007; Yakimov et al., 2007). Au contraire certaines espèces telles que *Marinobacter spp*. présentent une certaine polyvalence dans l'utilisation des composés hydrocarbonés (Yakimov et al., 2007).

Quantifier les taux de biodégradation associés aux déversements de pétrole dans le milieu marin est complexe. Plusieurs études ont permis de mettre en évidence certains paramètres physico-chimiques jouant un rôle dans la transformation des hydrocarbures par le bactérioplancton. D'abord, les conditions de turbulence du milieu vont jouer un rôle dans la dissolution et l'émulsification du pétrole, favorisant ainsi la biodégradation (Atlas, 1981). La température est un des paramètres majeurs limitant de la biodégradation. À de faibles températures ($\leq 5°C$), la diminution de l'activité métabolique de ces microorganismes limite leur croissance et engendre une réduction notable du taux de dégradation (Mulkins-Phillips and Stewart, 1974; Atlas and Bartha, 1972). Enfin, pour assimiler les HC, ces bactéries aérobies spécifiques sont dépendantes de la concentration en oxygène dissout et en éléments nutritifs du milieu. À la suite de l'accident de Deepwater Horizon dans le golfe du Mexique, des anomalies de concentration en oxygène dissout ont été observées au niveau de la plume d'hydrocarbures sans toutefois engendrer de phénomène d'hypoxie (Valentine et al., 2012; King et al., 2015). De nombreuses études considèrent le phosphore et l'azote comme éléments limitants dans le processus de biodégradation (Atlas and Bartha, 1972; Horowitz and Atlas, 1977). Néanmoins, lorsque les hydrocarbures se retrouvent sous forme dissoute, cette limitation n'est plus observée (Atlas, 1981; Shiller and Joung, 2012).

La présence d'hydrocarbures dans le milieu marin induit des changements dans la structure des communautés planctoniques. Alors, qu'un nombre important d'études ont permis de mesurer en laboratoire les effets directs de ces composés sur certains groupes ou assemblages d'organismes, la quantification *in situ* des processus biogéochimiques qui se produisent dans la colonne d'eau lors d'un déversement accidentel reste complexe car elle nécessite une bonne connaissance de la dynamique de l'écosystème dans son état non perturbé et un déploiement important de moyens techniques.

À partir des données de la littérature scientifique et des données de la mission PROMESse, nous tenterons de modéliser un déversement chronique d'hydrocarbures ainsi que la réponse planctonique à cette perturbation dans l'écoystème côtier du GSJ. La décision de simuler une pollution chronique dans le cadre de cette étude a été prise à la suite de différents tests de simulations reliés à la durée, la profondeur ou encore la période de contamination. Le scénario de type chronique décrit dans la section 1.3 a été choisi parce qu'il correspondait le mieux à la structure unidimensionnelle du modèle utilisé, mais aussi parce qu'il représentait un scénario éventuel de contamination provenant d'une plateforme "Offshore".

Objectifs

L'objectif principal de ce projet est d'étudier la dynamique du plancton marin et sa réponse à une contamination chronique par les hydrocarbures dans des conditions contrastantes de mélange (i.e., de part et d'autre d'un front de marée). Pour cela, trois sous-objectifs seront poursuivis :

1. Étudier la dynamique du plancton du GSJ à l'aide d'un modèle biogéochimique (adapté de Fasham et al. (1990)) couplé à un modèle de mélange vertical turbulent unidimensionnel de la colonne d'eau (GOTM).

2. Caractériser la réponse des communautés phyto-, zoo- et bactérioplanctoniques du GSJ à une contamination chronique par les hydrocarbures.
3. Comparer la réponse de chaque communauté dans deux régimes de mélange caractéristiques du GSJ, l'un fortement stratifié et l'autre bien mélangé, de part et d'autre du front de marée observable au sud-est du golfe.

L'article 1 présenté dans ce mémoire est composé d'une introduction présentant le cadre d'étude ainsi que la littérature scientifique utilisée pour paramétriser le modèle unidimensionel. Cette paramétrisation est d'abord décrite dans son aspect hydrodynamique puis comparée à certaines données récoltés durant la mission PROMESse. Par la suite, la description du modèle biogéochimique configuré englobe les modifications apportées à sa structure dans le but de simuler les effets des hydrocarbures sur la structure du système planctonique du GSJ. Avant la description des résultats, une sous-section présente l'organisation des différentes expériences réalisées lors de cette étude.

ARTICLE 1

EFFECTS OF A CHRONIC OIL SPILL ON THE PLANKTONIC SYSTEM IN THE SAN JORGE GULF, ARGENTINA: A ONE VERTICAL DIMENSION MODELLING APPROACH

Abstract

Coastal waters close to areas of oil exploitation might be susceptible to major pollution events. This could be the case in San Jorge Gulf (SJG), in Argentinian Patagonia, which is known for its high biological productivity. To understand the dynamics of the plankton ecosystem under several scenarios of hydrocarbon (HC) contamination, we present an eleven compartments biogeochemical model coupled to a turbulence model in which we parameterized the main physical and biological processes related to HC contamination, such as biodegradation, growth and mortality of phyto-, zoo- and bacterioplankton. The planktonic response to several levels of HC contamination is studied for two physically contrasting environments found in the SJG, a tidally well-mixed and a stratified water column. Results show increasing phyto- and bacterioplankton biomass with increasing concentrations of HC, which in turn produce more detritus. Zooplankton communities seem to respond differently depending on HC concentration, with major indirect changes occurring in the different size classes. Effects on biological compartments seem to be stronger in the stratified than in the well-mixed environment.

1.1 Introduction

Along the Argentinian coast, particularly within the San Jorge Gulf (SJG), oil production is the main economic resource since the beginning of the 20th century and accounts for nearly half of the total country production (Ministerio de Energía y Minería, 2016). Offshore exploration and extraction of this resource poses a risk on the marine ecosystem. It is therefore essential to understand the physical and biological dynamics of this region of the patagonian shelf. The SJG is exposed to strong sustained westerly winds throughout the year and strong semi-diurnal tidal currents, and characterized by a counterclockwise average circulation (Glorioso and Simpson, 1994; Glorioso and Flather, 1995; Palma et al., 2004). In the south-eastern shallow ($\leq$ 80 m) area of the SJG, there is significant turbulent mixing produced by the bottom friction of strong tidal currents (Glorioso and Flather, 1995). This phenomenon allows the maintenance of a permanent, mainly tidally-induced frontal zone in this particular region of the Gulf (Glorioso and Flather, 1997; Palma et al., 2004; Carbajal et al., forthcoming; Flores-Melo et al., forthcoming), also confirmed by sharp horizontal gradients in satellite observations of temperature and chlorophyll-*a* concentrations (Acha et al., 2004; Rivas et al., 2006; Glembocki et al., 2015). High production areas are often associated with high horizontal density gradients, where turbulence plays a role not only in the availability of nutrients in the euphotic zone but also in the distribution of phytoplankton biomass (Flores-Melo et al., forthcoming).

Studying and quantifying the effects of hydrocarbons (HC) on planktonic assemblages is difficult to achieve *in situ*. Micro- and mesocosm experiments provide ways to target the direct effects of contamination on plankton by controlling the experimental conditions such as nutrient concentration, temperature and light intensity, affecting growth, mortality and distribution of the organisms. However, because coupled biological-physical processes are non-linear, the influence of physical factors cannot be accounted for in this

kind of studies.

Dissolved HC, especially Polycyclic Aromatic Hydrocarbons (PAHs), contributing up to 60% of the total oil composition (Brown et al., 2011) have the most negative effect on marine organisms. The hydrophobic nature of these compounds and their bioavailability, once dissolved in the marine environment, promotes their adsorption by marine organisms increasing their mortality by simple toxicity or by decreasing their physiological activity (Anderson et al., 1974). On the other hand, specific strains of bacterioplankton participate in one of the most persistent disaggregation processes found during a HC contamination (Beazley et al., 2012): biodegradation. Since the early 20th century the study of their genome made it possible to isolate nearly 200 genera capable of degrading HC (Prince et al., 2003; Head et al., 2006; Cappello et al., 2007). In the marine environment, bacterioplankton exhibit significant changes of community structure and biomass following an oil spill (Hazen et al., 2010; Dubinsky et al., 2013). These marine bacteria (known as Obligate HC-Degrading Bacteria (OHCB, Yakimov et al. (2007)) are ubiquitous at very low concentrations in the water column and are characterized by high substrate specificity.

Besides, in order to assimilate HC through fast growth rates, bacterioplankton depends on the concentration of dissolved oxygen and nutrients present in the water column (Valentine et al., 2012; King et al., 2015). For example, phosphorus- and nitrogen-based compounds seem to act as regulators of biodegradation processes (Atlas and Bartha, 1972; Horowitz and Atlas, 1977; Atlas, 1981), thus limiting or promoting HC incorporation into pelagic carbon biomass (Shiller and Joung, 2012). However, the scarcity of informations concerning the limiting nutrient forms and their related consumption makes it difficult to estimate precise biodegradation rates associated with HC spreading in seawater.

Phytoplankton is the class of microorganisms presenting the highest variability of

responses after HC contamination. From an ecotoxicological perspective, some phytoplankton groups appear to be more affected than others at equivalent concentrations. This is the case of diatoms, which may undergo a sharp decrease in growth (Hsiao, 1976; Nayar et al., 2005), attributable to the siliceous composition of their wall that significantly adsorbs and accumulates PAHs (Siron et al., 1996; Sargian et al., 2007). However, other results show a stimulation of phytoplankton growth at low concentrations of dissolved portion of HC (Gordon and Prouse, 1973; Dunstan et al., 1975; Hsiao et al., 1978; González et al., 2013). The mechanisms associated with an increase in photosynthetic activity are poorly understood and lead to several hypotheses: Baker (1971) and Cabioch et al. (1981) results suggest that an extra nutrient uptake occurs from the degradation of dead organisms by HC toxicity.

In the presence of HC, all major zooplankton groups appear to be affected, and different effects are observed depending on species and HC concentrations. Almeda et al. (2013) observed copepod mortality of 96% after 16 hours with concentrations of 100 μl.L^{-1} of PAHs. They also calculated a mean lethal concentration LC_{50} of 31.4 μl.L^{-1}. Narcosis is another effect observed in laboratory experiments (Barata et al., 2005). This process, which is still poorly understood, is described by Almeda et al. (2013) who show that low concentrations (10 μl.L^{-1} to 20 μl.L^{-1}) considerably decrease the metabolism and displacement capacities of copepods up to the death of the organism.

Modelling makes it possible to simulate the biogeochemical dynamics of pelagic systems in realistic physical settings as well as the effects of contamination. The General Ocean Turbulence Model (GOTM) developed by Burchard et al. (2006) is a vertical one-dimensional (1D) model of turbulence to which a biogeochemical model of Nitrate-Phytoplankton-Zooplankton type (i.e. as Fasham et al. (1990)) can be coupled. The simulations can take into account the annual evolution of the mixing depth and emphasize the

importance of the microbial loop in the renewal of nitrogen available for primary production. The effect of contaminants on the biological compartments can be further parameterized, allowing for a complete, physical and biological interpretation of the effects of pollutants on plankton. Previous studies have simulated the behaviour of HC in the marine environment (Reed et al., 1999), but only few models measure their impact on the biogeochemical dynamics of the planktonic system (Gin et al., 2001; Valentine et al., 2012; González et al., 2013).

In this study, we will combine data from the scientific literature and from the 2014 PROMESse cruise in the SJG (Carbajal et al., forthcoming; Flores-Melo et al., forthcoming; Latorre et al., forthcoming) to simulate a "Offshore" oil incident and study the response of plankton to a chronic HC contamination in a turbulent environment by means of a one-dimensional biogeochemical-physical modelling approach. Two mixing regimes typical of the south-eastern frontal region of the SJG will be compared: a seasonally stratified zone and a shallower tidally well-mixed zone.

1.2 Model description

1.2.1 Physical model and description

We used the GOTM coupled to a biogeochemical model (see section 1.2.2) to resolve the advection-diffusion equation on the vertical dimension, assuming that state variables are horizontally homogeneous and both mean and turbulent transport are driven by wind, buoyancy fluxes and shear production. However, transport of quantity from advection is not taken into account.

The density and hydrographic conditions were characterized during the PROMESse cruise at multiple CTD (Conductivity, Temperature and Depth) stations and by the use

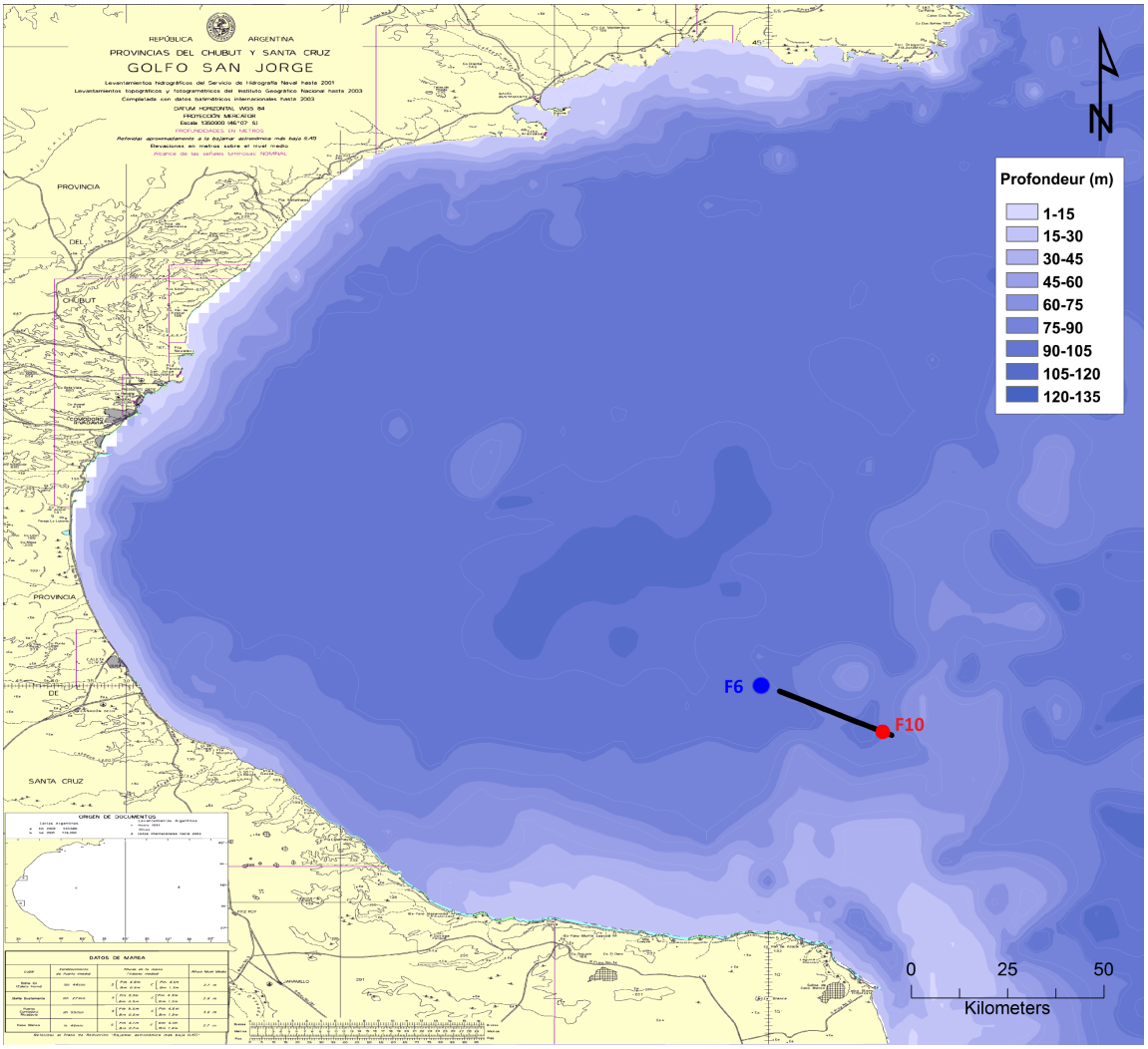

Figure 1. Bathymetric map of the San Jorge Gulf with reference stations identifying the shallower (F10) and the deeper (F6) region of the southeastern frontal area (source : Servicio de Hidrografía Naval)

of a remotely operated towed vehicle Scanfish®. Scanfish transects were conducted to precisely locate the tidal front, and CTD stations at each side of the front were chosen as geographical references (Figure 1) (see a complete description in Flores-Melo et al.

(forthcoming); Carbajal et al. (forthcoming)). Initial profiles were set as two layers profiles for salinity and temperature (Table 1).

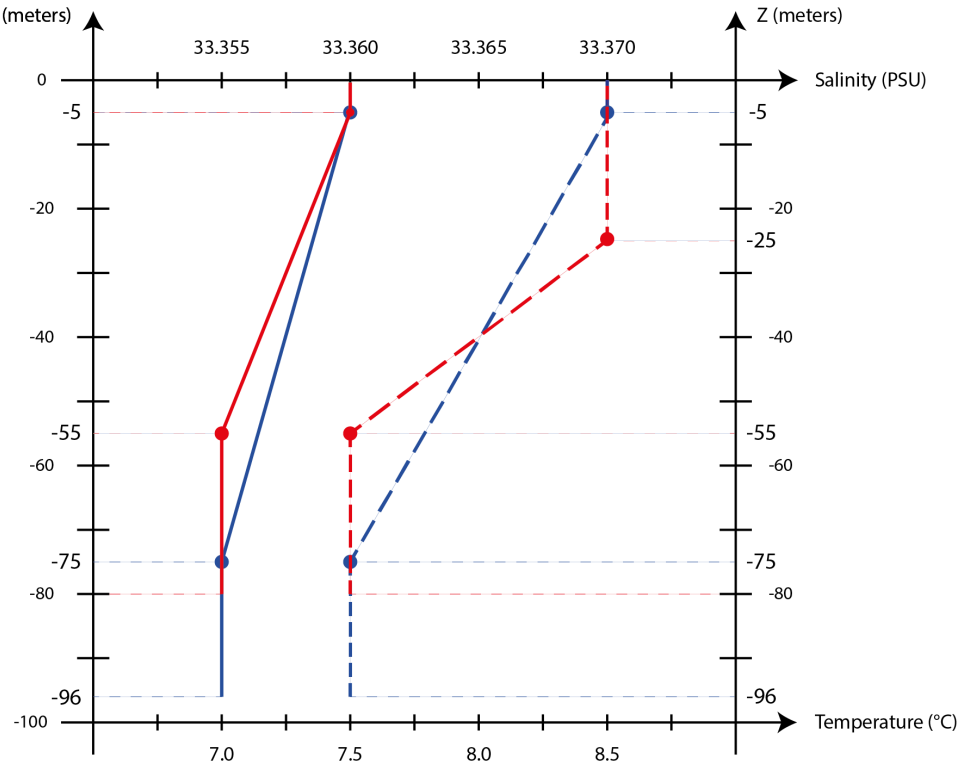

Param. \ Exp.	Stratified	Well-mixed
Temperature	—	—
Salinity	- - -	- - -
Depth | z | (in m)	96	80
Number of levels (vertical resolution)	48	12
Amplitude of elevation gradient	2.5×10^{-7}	2.5×10^{-5}
Time steps (in sec)	120	80

Figure 2. Physical environment parameters (Param.), simulation conditions and initial profiles of salinity and temperature (in °C) applied to the stratified **(Blue curve)** and the well-mixed **(Red curve)** experiment (Exp.).

Model simulations start on August 1, 2012 and ends on July 31, 2015 in order to initialize the model, 12 months before the contamination experiment (see section 1.3). We chose to begin our simulations during the austral winter to evaluate the interannual evolution of variables and the effects of HC on the austral spring and autumn phytoplankton blooms. Atmospheric forcing was obtained from European Centre for Medium-Range Weather Forecasts (ECMWF) reanalysis datasets in 6-hourly intervals with a spatial resolution of 80 Km. Longitude and Latitude were set in GOTM using geographical positions acquired during the Leg_2 of the PROMESse cruise. The stratified experiment (46°29'39.48" S; 66°0'55.079" O) and well-mixed experiment (46°35'49.499" S; 65° 46'49.079" O), separated by 21.4 Km, correspond to stations F6 and F10, respectively.

For each experiments, a specific barotropic mean flow representing the pressure-gradient was forced by prescribing an external sea surface elevation gradient oscillating at the M_2 frequency, the dominant tidal constituent in the area (Palma et al., 2004). The amplitudes of this gradient (Figure 2) were tuned to obtain current velocity of the order of those measured by the onboard ADCP during the PROMESse cruise, and derived from Palma et al. (2004) results .

Figure 3 presents temperature, heat diffusivity and horizontal current speeds for each experiment as basic physical properties to couple with the biogeochemical model. Noticeable differences between the simulated and observed temperature profiles (Figures 3a and 3b) can be explained by the absence of horizontal advection not considered in the one-dimensional structure of the GOTM.

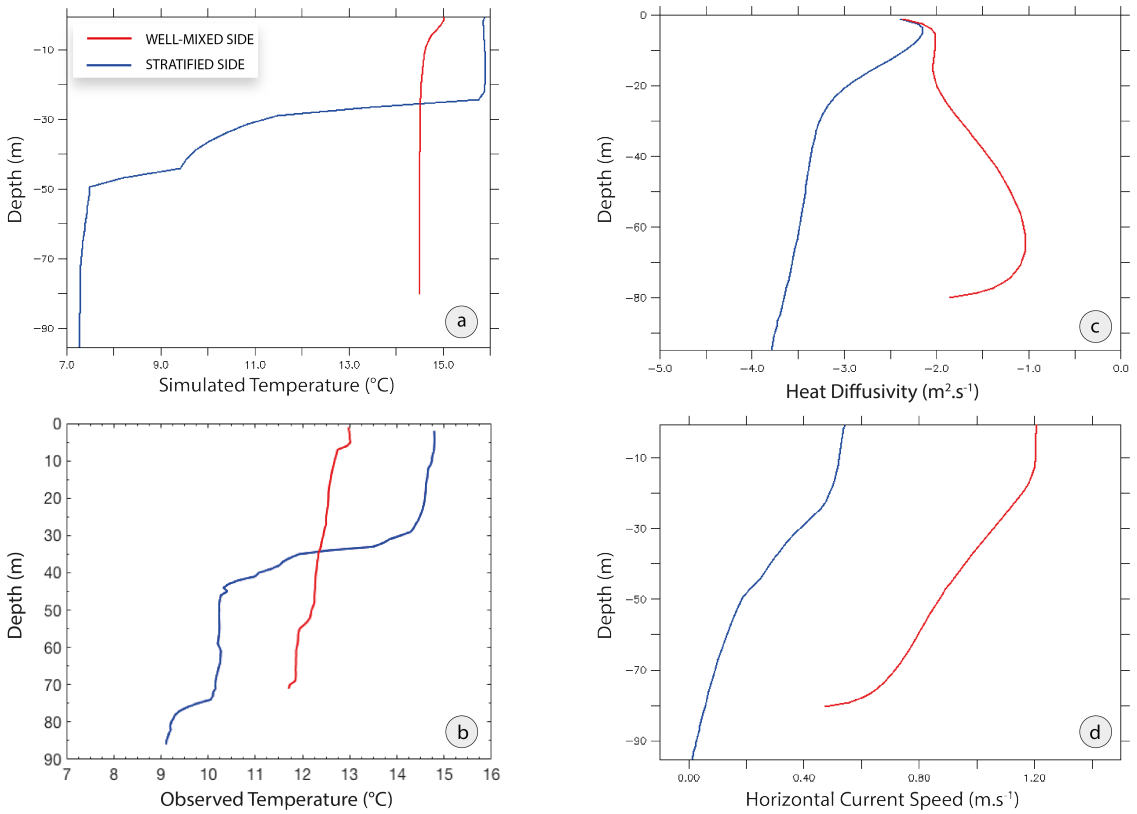

Figure 3. Vertical profiles of **(a)** simulated temperature (in °C) and **(b)** observed temperature (in °C) during the PROMESse cruse at stations F6 and F10 on the 8th of February 2014, **(c)** yearly averaged simulated heat diffusivity (in m^2s^{-1}) and yearly averaged simulated horizontal ($x-$ and $y-$) current speeds (ms^{-1}) for the stratified **(Blue curve)** and the well-mixed **(Red curve)** experiments.

1.2.2 Biogeochemical model and configuration

The biogeochemical model is composed of 11 compartments with a Nitrate - Phytoplankton - Zooplankton - Detritus (NPZD) based structure connected to a microbial loop, thus reproducing nitrogen recycling from labile dissolved organic nitrogen (LDON) to ammonium (NH_4^+) (Figure 4). Because nitrogen is the limiting element in most of marine

ecosystems (Howarth, 1988), understanding its dynamics is an essential prerequisite to describe the carbon cycle (Fasham et al., 1990). Each biogeochemical variable is expressed in nitrogen concentrations (mmol N m^{-3}).

The biological super-compartments (bacteria, phytoplankton and zooplankton) are each divided in two compartments. The bacterial super-compartment includes one bacterial compartment (BAC1) representing the bacterioplankton involved in the natural microbial loop, responsible for nitrogen recycling of detritus via LDON into ammonium only, and a second, "oil-degrading" bacterial compartment (BAC2, representing "OHCB" strains), found in high concentration in oil-contaminated waters (see section 1.2.3.1).

Two phytoplankton groups are considered to represent the main sizes of organisms found in SJG (diatoms and flagellates; (Latorre et al., forthcoming)). In order to understand indirect effects of HC on this super-compartment, both groups were parameterized with the same growth rates, initial concentrations, and settling velocities. Differences between diatoms (DIA) and flagellates (FLA) were only parameterised for mortality, simulated through zooplankton grazing specificity and transformation into detritus. An exudation factor reproduces the transfer of nitrogen to the LDON. Given the high variability of HC effects on phytoplankton, no direct effect was parameterized and only the indirect effects were taken into consideration.

Two zooplankton classes represent micro- (MCZ) and mesozooplankton (MSZ), with grazing preferences on diatoms, flagellates, detritus, bacteria, and diatoms, flagellates, detritus, microzooplankton, respectively. Zooplankton loss by exudation, natural mortality and mortality by HC toxicity are the three sink terms leading to fluxes towards the ammonium, LDON and detritus compartments (Equations (B.3.1), (B.3.2), (B.3.5), (B.3.6), (B.3.7) and (B.3.8) in Appendix 2).

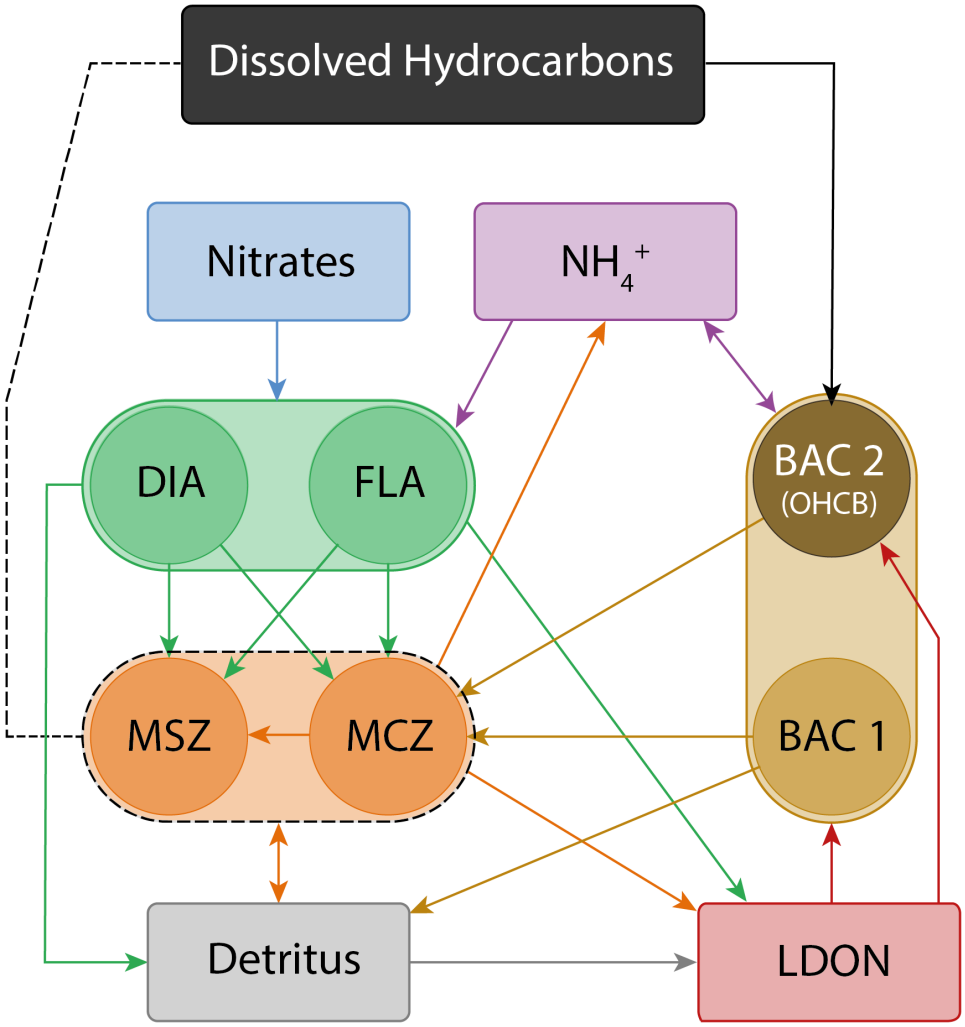

Figure 4. General structure of the biogeochemical model : Dissolved Hydrocarbons, Nitrates, Ammonium (NH_4^+), Diatoms (DIA), Flagellates (FLA), Microzooplankton (MCZ), Mesozooplankton (MSZ), Traditional Bacteria ($BAC1$), Obligate Hydrocarbon degrading Bacteria ($BAC2$), Labile Dissolved Organic Nitrogen ($LDON$) and Detritus. Dashed lines illustrate the direct effects HC on biological compartments. Each straight-line arrow represents a flux and each compartment a concentration in mmol N m^{-3}.

Nitrate is initialized at the beginning of the simulations at 15 mmol N m^{-3} in the upper layer (0-30 m) and 30 mmol N m^{-3} in the bottom layer (-66 m to bottom) and a relaxation time of 365 days is applied to the bottom layer only. Ammonium is initialized at the beginning of the simulations at 0.20 mmol N m^{-3} in the upper layer (0-25 m) and 0.01 mmol N m^{-3} in the bottom layer (-35 m to bottom). In order to set low concentrations of ammonium during the entire simulation, a relaxation time of 3 months is applied to the two layers. The ammonium transformation to nitrate is an existing flux included into the model. Nevertheless, because the nitrate and ammonium compartments are parameterized with relaxation times, we decided to keep the nitrification rate to 0.0 day^{-1}.

LDON accounts for the portion of broken molecules identified within the dissolved organic nitrogen pool that can be rapidly used by bacteria to enhance remineralisation. This compartment is supplied by the six biological compartments (DIA, FLA, MSZ, MCZ, BAC1 and BAC2) through exudation and by breakdown of sinking detritus.

1.2.3 Parametrization of HC effects

To simulate the presence of HC in GOTM, we considered a new variable corresponding to the portion of HC dissolved in seawater resulting from weathering processes. As literature suggests, the dissolved portion, also called “water accommodated fraction” is considered to be the most toxic HC state for marine biota (Anderson et al., 1974). Parameterization of direct effects related to HC toxicity is applied to the zooplankton supercompartment only (see section 1.2.3.2). Therefore, effects on phytoplankton dynamics after HC contamination are only indirect effects.

1.2.3.1 Parametrization of biodegradation

Biodegradation of oil spill compounds involves a large number of specific organisms and biochemical processes. Thus, quantifying the carbon transfer to the planktonic food web remains a challenging task. The choice of integrating this type of processes within the GOTM structure came with several interrogations. Because the compounds contained into the extracted oil are composed of ≤ 1 % of nitrogen (Musser et al., 1999; Brown et al., 2011; Petroleum HPV Testing Group, 2011; Reddy et al., 2012), establishing realistic HC consumption rates through C:N ratios was not possible. Therefore, we chose concentrations within the 5 to 100 μl.L^{-1} range (Almeda et al., 2013) and converted this equivalent to mmol N m^{-3} following a 1:1 HC to nitrogen ratio (see section 1.3).

Consequently, the flux from the HC to OHC Bacterial compartment was the only biologically mediated loss for HC in the model, allowing for the incorporation of HC into the biogeochemical pelagic environment (Equation (B.5.3)). Maximal HC uptake rate vb_2 for this flux was chosen following Burchard et al. (2006) study. Here, we applied the same value as vb_2 , equal to 1.2 day^{-1}, representing maximal ammonium uptake by bacteria (BAC1).

$$C_{11,6} = vb_2 \; min_{HL} \; (C_6 + C_5^{min}) \tag{B.5.3}$$

Where C_{11} is the hydrocarbon concentration in mmol N m^{-3}, C_6 is the Obligate Hydrocarbon Bacterial concentration in mmol N m^{-3}, vb_2 is the maximal uptake rate of the "OHCB" compartment in day^{-1}, C_5^{min} is the minimal bacterial concentration in mmol N m^{-3} and min_{HL} is the minimal HC to LDON uptake ratio for OHC bacteria (B.6.2).

Biodegradation also involves the consumption of nitrogen-based compounds. However, the form of nitrogen utilised by OHC Bacteria in these processes is not known (see

section 1.1). Therefore, we made the hypothesis that the LDON compartment, the most bioavailable form consumed by bacteria, applies a co-limitation on HC consumption. HC directly stimulates OHCB bacterioplankton (BAC2) but they compete for substrate with BAC1, therefore affecting the whole bacterioplankton super-compartment. Equation (B.6.2) describes the minimal HC to LDON uptake ratio for the OHCB compartment (Appendix 2).

$$min_{HL} = min\left(\frac{C_{11}}{K_{10} + C_{11}}, \frac{C_9}{K_4 + C_9}\right) \tag{B.6.2}$$

Where C_{11} is the Hydrocarbon concentration in mmol N m^{-3}, C_9 is the Labile Dissolved Organic Nitrogen concentration in mmol N m^{-3}, K_4 is the half saturation constant of traditional bacteria uptake in mmol N m^{-3} and K_{10} is the half saturation constant of "OHC Bacteria" uptake in mmol N m^{-3}.

1.2.3.2 Effects of HC on zooplankton mortality

Micro- and mesocosms experiences results show different but directly noticeable effects of HC on the survival of zooplankton species. Almeda et al. (2013) show that copepod species seem to be strongly affected and propose a sigmoid numerical model of mortality with increasing HC concentration. Therefore, we integrated this relationship between mesozooplankton mortality and the HC concentration to the existing natural mortality rates μ_{21} and μ_{22} (Equations (B.3.3), (B.3.4)). Since no specific mortality rates were found for microzooplankton species, we applied the same HC toxicity to micro- and mesozooplankton (Equations (B.3.1), (B.3.2)).

$$\mu_{21}^{HC} = \mu_{21} + (\mu_{21}^{max} - \mu_{21})\left(\frac{(C_{11})^5 + (C_{11}^{min})^5}{(K_6^{HC})^5}\right) \tag{B.3.3}$$

$$\mu_{22}^{HC} = \mu_{21}^{HC} \tag{B.3.4}$$

Where μ_{21}^{HC} is the microzooplankton mortality rate from HC toxicity in day^{-1}, μ_{21} is the microzooplankton mortality rate in day^{-1}, μ_{21}^{max} is the maximal microzooplankton mortality rate from HC toxicity in day^{-1}, μ_{22}^{HC} is the mesozooplankton mortality rate from HC toxicity in day^{-1}, C_{11} is the Hydrocarbon concentration in mmol N m^{-3} and K_6^{HC} is the half saturation constant of micro- and mesozooplankton loss by HC toxicity in mmol N m^{-3}.

$$C_{3,7} = (1-\beta_z)\,(g_2^{max}\, r_{24}\, {C_6}^2\, Fac_2) + (1-\epsilon-\delta)\,\mu_{21}^{HC}\,\frac{(C_3 + C_3^{min})}{K_6 + (C_3 + C_3^{min})}\,C_3 \qquad \text{(B.3.1)}$$

$$C_{4,7} = (1-\epsilon-\delta)\,\mu_{22}^{HC}\,\frac{(C_4 + C_3^{min})}{K_6 + (C_4 + C_3^{min})}\,C_4 \qquad \text{(B.3.2)}$$

where C_3 is the microzooplankton concentration in mmol N m^{-3}, C_4 is the mesozooplankton concentration in mmol N m^{-3}, C_7 is the detritus concentration in mmol N m^{-3}, C_3^{min} is the minimal zooplankton concentration β is the grazing effeciency coeficient, ϵ is the fractional zooplankton loss of ammonium, δ is the fractional zooplantkon loss of LDON, Fac_2 is the mesozooplankton preference normalization factor (B.2.11), ρ_{24} is the mesozooplankton grazing preference on microzooplankton, g_1^{max} is the maximal microzooplankton ingestion rate in day^{-1}, g_2^{max} is the maximal mesozooplankton ingestion rate in day^{-1} and K_6 is the half saturation constant of micro- and mesozooplankton loss in mmol N m^{-3}.

A version of the complete biogeochemical code can be found following the above link : https://gitlasso.uqar.ca/dumoda01/gotm_ismer/blob/master/src/extras/bio/bio_gsj.F90

1.3 Chronic oil spill scenario

Because chronic oil spills account for the majority of HC pollution in seawater (Potters, 2013), we have chosen to simulate a chronic oil spill replicating an offshore oil leak. HC is incorporated to the system in a subsurface 5 m layer with a small relaxation time (7 days). In order to target the austral summer, start of contamination was set from August 1, 2013 to July 31, 2014. To evaluate different responses of the planktonic system, we simulated one control and 3 levels of contamination (0, 10, 20 and 50 mmol N m^{-3})(Table 1). Finally, each simulation was applied to different physical regimes studied and parameterized in the physical model (stratified and well-mixed). For example, **CST**$_{00}$ will be referenced as the control simulation in the **ST**ratified experiment using the latest **C**omplete version of the biogeochemical model.

Simulation reference	Experiment conditions	Model version	Perturbation concentration (in mmol N m^{-3})
CST$_{00}$	Stratified	Complete	00
CST$_{10}$	Stratified	Complete	10
CST$_{20}$	Stratified	Complete	20
CST$_{50}$	Stratified	Complete	50
CWM$_{00}$	Well-mixed	Complete	00
CWM$_{10}$	Well-mixed	Complete	10
CWM$_{20}$	Well-mixed	Complete	20
CWM$_{50}$	Well-mixed	Complete	50

Table 1. References for the simulations used and described in this study

1.4 Results and discussion

1.4.1 Physical environment dynamics

As it occurs in the SJG (Glorioso and Simpson, 1994; Glorioso and Flather, 1995; Palma et al., 2004), in the model, wind stress and tidally induced horizontal current speeds are the only contributors to vertical distribution of biogeochemical concentrations. Regardless of the experiment, wind stress shows a seasonal pattern with stronger average values during the austral winter. However, in the stratified experiment, which aims at reproducing the stratified side of the tidal front in the south-eastern region of the SJG, episodic wind events seem to have a strong influence on upper layer mixing (Figure 5a and 6a), allowing the deepening of biotic and abiotic variables at weekly timescales.

Temperature, the driving conservative property for stratification at the SJG latitude (Krepper and Rivas, 1979), shows a marked two-layer stratification pattern in the stratified experiment from November 2013 to April 2014 (Figure 5b). The presence of a seasonal thermocline during spring and summer is confirmed by Akselman and Carreto (1996) results. Moreover, satellite observations of sea surface temperature show similar values at the southeastern stratified region of the SJG (Glembocki et al., 2015).

Whilst interesting spatial variations can be observed throughout the stratified experiment results, temperature for the well-mixed experiment is almost vertically constant. Maximum temperatures range from 6.6 to 15.8 °C in September and March respectively (Figure 6b). These values are in accordance with Glembocki et al. (2015) results. Moreover, Carreto et al. (2007) showed that vertically homogeneous conditions are found in the southeastern area of the SJG during spring and summer.

In both experiments, salinity does not show vertical stratification throughout the

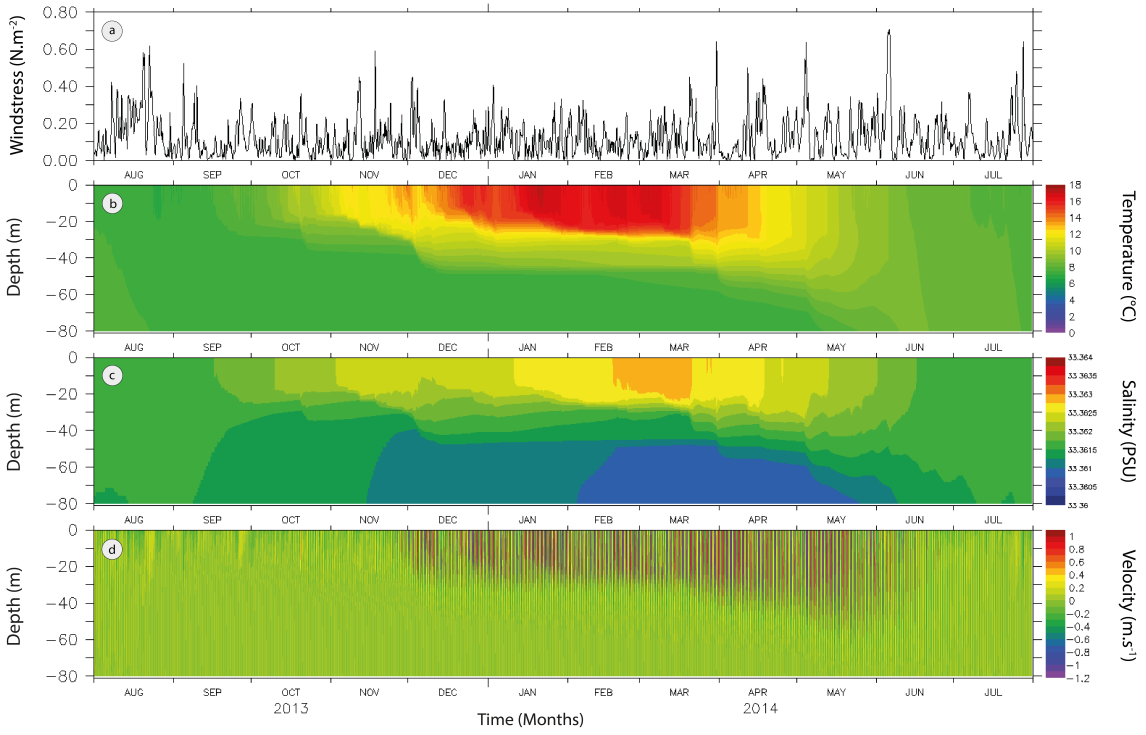

Figure 5. 2013/2014 Annual cycle of **(a)** Wind Stress at sea surface calculated from ECMWF reanalysis database (in $N.m^{-2}$), **(b)** Simulated Temperature **(c)** Simulated Salinity, and **(d)** Simulated horizontal velocity U for the stratified experiment.

entire year (Figure 5c and 6c). This pattern is associated with the intrusion of the homogeneous Magellan Plume at the south of the SJG (Krepper and Rivas, 1979; Palma and Matano, 2012).

Maximal current speed amplitudes are found in the upper 20 meters, decreasing towards the bottom of the water column (Figure 6e). This result can be explained by the turbulent forcing regime applied in this experiment throughout the amplitude of the external pressure gradient generated by M_2 tidal constituent (Figure 2). These homogeneous conditions agree with (Krepper and Rivas, 1979) results, pointing that surface wind stress

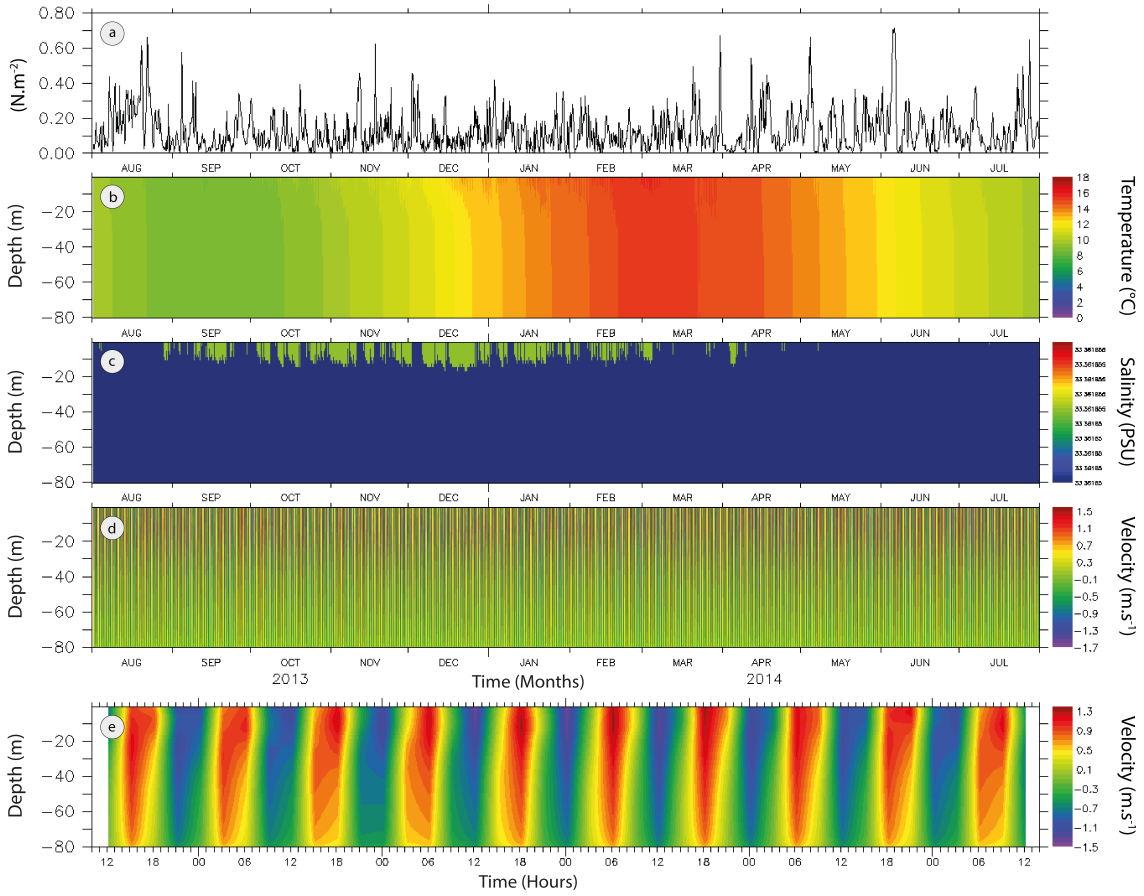

Figure 6. 2013/2014 Annual cycle of **(a)** Wind Stress at sea surface calculated from ECMCWF reanalysis database (in $N.m^{-2}$), **(b)** Simulated Temperature, **(c)** Simulated Salinity, **(d)** Simulated U horizontal velocity and ,**(e)** Simulated U horizontal velocity with X-Axis emphasis from the 28th of January to the 3rd of February 2014, for the well-mixed experiment.

and strong tidally-induced mixing leading to noticeable bottom friction are the main external contributors to the vorticity balance in this region of the south-western Atlantic Shelf.

It should be noted that, for the control simulations in both experiments, ammonium and nitrate relaxation times and values (see section 1.2.2), induce a decrease in nitrogen

towards the end of the simulations resulting in non-conservativity of the model. However, when the relaxation is not applied, the model remains conservative over the entire simulations (**CST** and **CWM**).

1.4.2 Distribution of HC

In the stratified experiment, vertical distribution of dissolved HC follows a summer two-layer stratification close to the thermocline depth (Figure 7a, 7b and 7c). During winter, vertical mixing allows the deepening of low hydrocarbon concentrations, thus reaching the bottom of the water column particularly between August and October 2013. In the well-mixed experiment, almost vertically homogeneous concentrations can be observed from the beginning of the simulation for all levels of perturbation with subtle differences within the upper 30 m (Figure 7d, 7e and 7f).

In the stratified experiment, at the lowest level of perturbation experiment ($\mathbf{CST}_{10}$) (Figure 7a), HC concentrations range from 1 to a maximum of 6 mmol N m^{-3}, last measurable on September 29th - 30th, 2013 between 0 and 20 m. From the end of August to mid-October 2013, 2 mmol N m^{-3} are found between 50 and 80 m. The system gets cleared of HC on November 16th 2013. However, on the first week of May 2014, low concentrations appear again between 0 and 40 m until the end of July 2014.

In the well-mixed experiment (Figure 7d), values ranging from 4 - 5 mmol N m^{-3} are found from late September to mid-October 2013. Thereafter, a quick reduction of the concentrations is followed by the disappearance of HC in the system 2 weeks earlier than in the stratified experiment, remaining without any HC until the end of the simulation.

At the highest level of perturbation (Figure 7c), contrasting results can be observed between the two experiments. First, in the stratified experiment, biodegradation processes

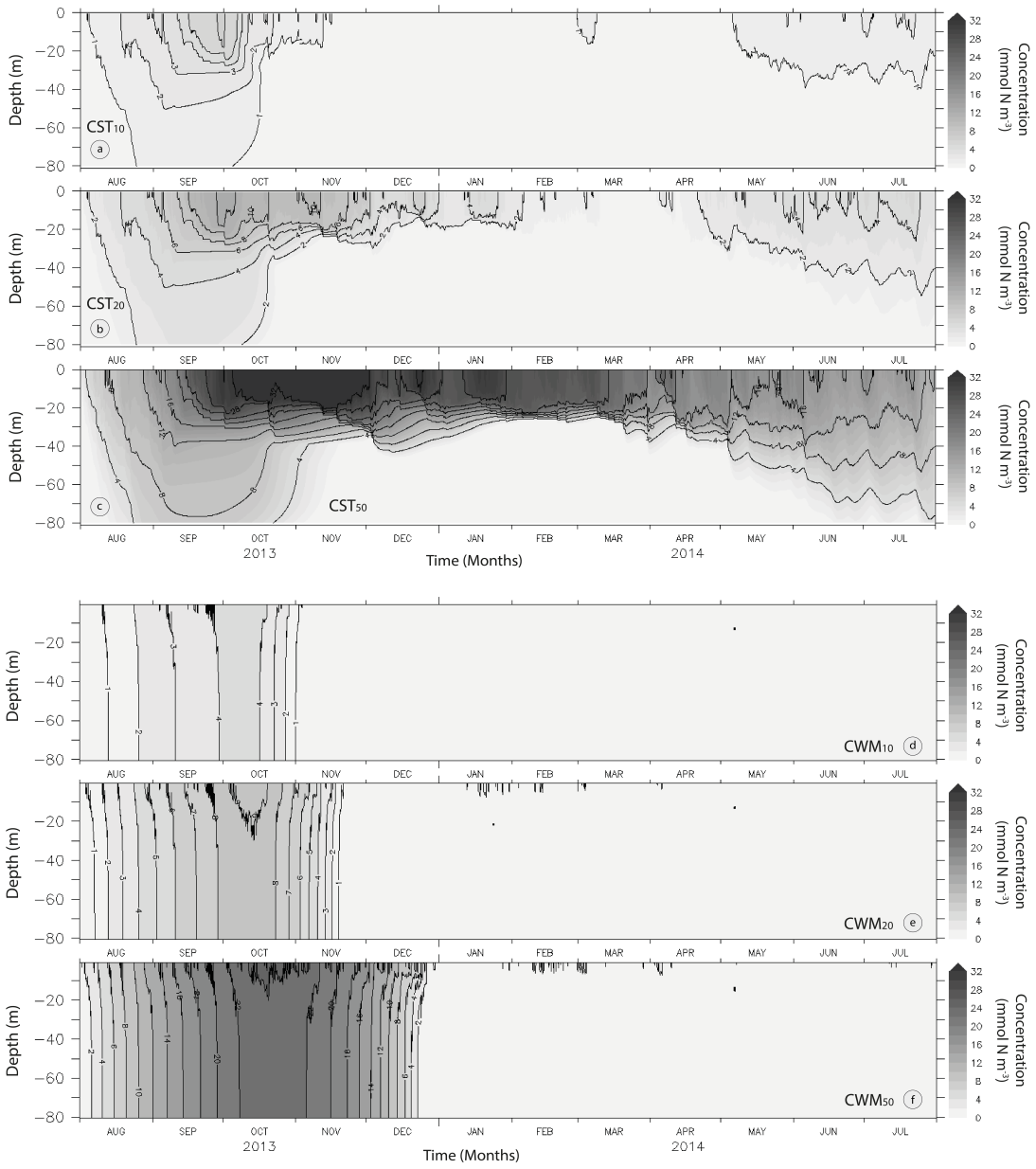

Figure 7. 2013/2014 annual cycle of Hydrocarbon concentration at 10 mmol N m^{-3}, 20 mmol N m^{-3} and 50 mmol N m^{-3} of contamination for the Stratified **(a)**, **(b)**, **(c)** and the Well-Mixed experiment **(d)**, **(e)**, **(f)**, respectively.

never seems thoroughly effective over the entire simulation and the maximal HC concentration at 32 mmol N m^{-3} remains from the first week of October to the first week of December 2013 between 0 and 20 m.

Conversely, in the well-mixed experiment (Figure 7f), most of the HC present has been degraded over the entire water column 5 months after the first contamination input. Moreover, maxima are significantly lower, with 24 mmol N m^{-3}, found from the first week of October to the first week of November 2013 from the surface to 22 m. These contrasting results, particularly at high concentrations show that different turbulent regimes have strong effects on the distribution and dilution of the contaminant. In the well-mixed experiment, a faster consumption of HC is associated to lower concentrations resulting in a more effective biodegradation occuring over the entire water column. On the other hand, in the stratified experiment, higher concentrations of HC only found above the thermocline during spring and summer reduce biodegradation (see section 1.4.4).

1.4.3 Effects of HC on abiotic compartments

In the control experiment $\mathbf{CWM}_{00}$, by mid-January 2014, 8 mmol N m^{-3} nitrate are still available, whilst this same value is reached earlier, in late October 2013, for $\mathbf{CWM}_{20}$. In the stratified experiment, $\mathbf{CST}_{00}$ and $\mathbf{CST}_{20}$ results show concentrations reaching 12.5 mmol N m^{-3} in the bottom layer (50 to 80 m) from mid-December 2013 to mid-May 2014. Between 0 and 20 m, minima between 0.5 and 2 mmol N m^{-3} are found from mid-December 2013 to the end of March 2014 for the $\mathbf{CST}_{00}$ simulation and from mid-October 2013 to the end of March 2014 for the $\mathbf{CST}_{20}$ simulation. These depletions are related to an earlier phytoplankton development (nitrate consumption) in the upper water column in the presence of HC (Figure 12b). However, studies conducted on the biogeochemistry of the Deepwater Horizon spill (DWHs) did not found correlations with the presence of a HC

plume and nitrate concentrations (Shiller and Joung, 2012; Dubinsky et al., 2013).

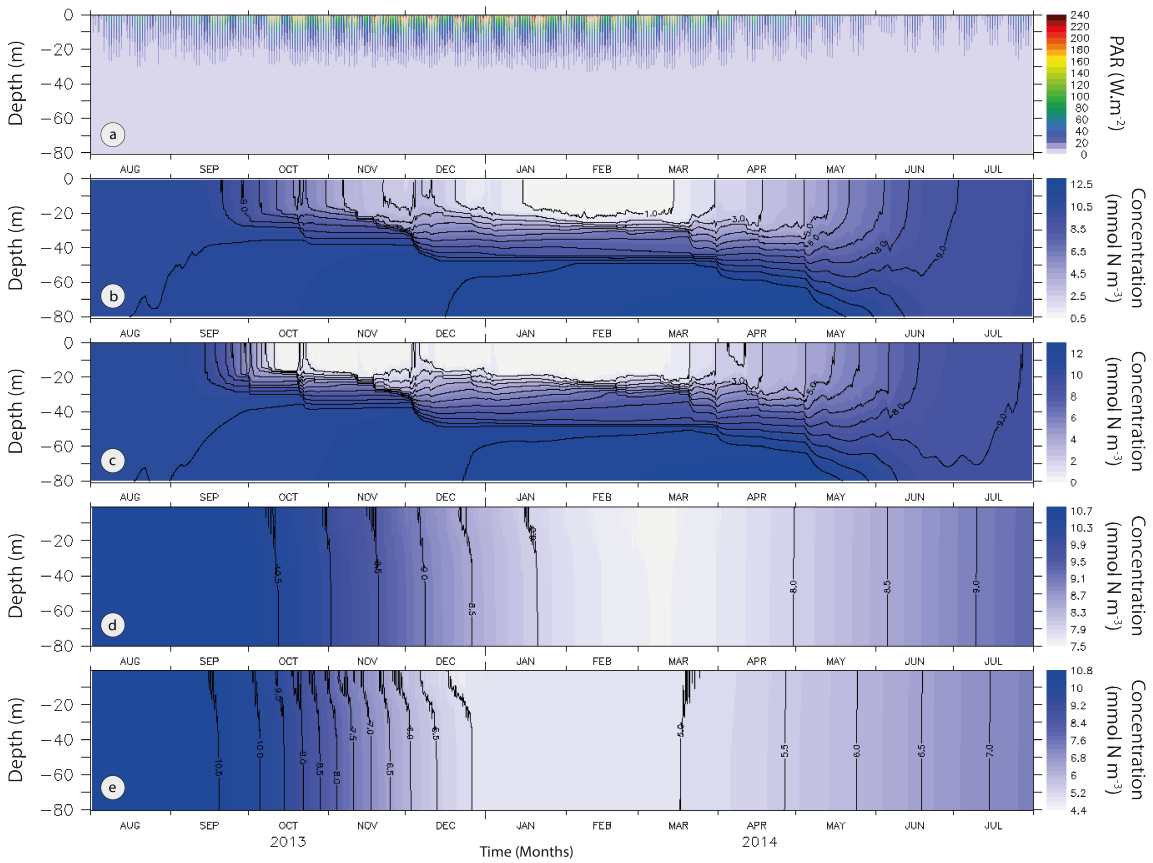

Figure 8. 2013/2014 annual cycle of **(a)** Simulated Photosynthetically Active Radiation (PAR) , Simulated Nitrate for the **(b)** $\mathbf{CST}_{00}$ **(c)** $\mathbf{CST}_{20}$ simulations. Simulated Nitrate for the **(d)** $\mathbf{CWM}_{00}$ and the **(e)** $\mathbf{CWM}_{20}$ simulations.

In comparison to the $\mathbf{CST}_{00}$ simulation, results from the stratified experiment reveal abnormally elevated concentrations of ammonium. $\mathbf{CST}_{10}$, $\mathbf{CST}_{20}$ and $\mathbf{CST}_{50}$ simulations present respectively values 2, 3 and 7 times higher than the control $\mathbf{CST}_{00}$ (Figure 9c). On April, 13, a maximum reaches 15 mmol N m^{-3} at 30 m for the $\mathbf{CST}_{20}$ simulation (Figure 9c). These values can be explained by a sustained bacterial activity below the thermocline (Figure 12d). During the same period, detritus vertical dynamics (Figure 10d)

follow a similar pattern, confirming the active microbial loop in the HC contaminated experiments. In contrast, above the thermocline, concentrations of ammonium ranging from 2 to 4 mmol N m^{-3} decrease to 0 mmol N m^{-3} in December 2013 and January 2014. At these depth, a significant growth of phytoplankton linked to the consumption of ammonium explains this depletion during summer.

In the well-mixed experiment, vertical detritus distribution follows a very homogeneous pattern. Results from simulation $\mathbf{CWM}_{20}$ show values 7 times higher than the control at the beginning of June 2014. In both experiment, increasing concentrations of ammonium starting at the end of summer 2014 are not consistent with Shiller and Joung (2012) who showed that ammonium and nitrite did not increase after the DWHs. Since nitrification is not considered in the model, ammonium is the compartment accumulating nitrogen from HC related to the intense growth of bacterioplankon (BAC1 and BAC2).

LDON, as part of the biodegradation process, shows interesting variations especially in the stratified experiment. In $\mathbf{CST}_{00}$, a slow depletion from 0.3 mmol N m^{-3} in October 2013 to 0.05 mmol N m^{-3} in May 2014 is evident between 0 and 80 m (Figure 9a). In $\mathbf{CST}_{20}$, a fast depletion (0.30 to 0.05 mmol N m^{-3}) characterized the 25 meters below the surface from the 12th of October 2013 to the end of March 2014 (Figure 9b). In the upper water column, this decrease of LDON concentration is clearly following the presence of HC (Figure 7c) and consequently, the augmentation of bacterial biomass (Figure 10a) from October to March, diminishing down to the absence of LDON in the upper 60 m in June 2014.

On the other hand, LDON concentrations do not show strong dependence on stratification. This vertical dynamic pattern is associated with exudation from phyto- and zooplankton increasing in the upper column until autumn, but also with the sinking and re-

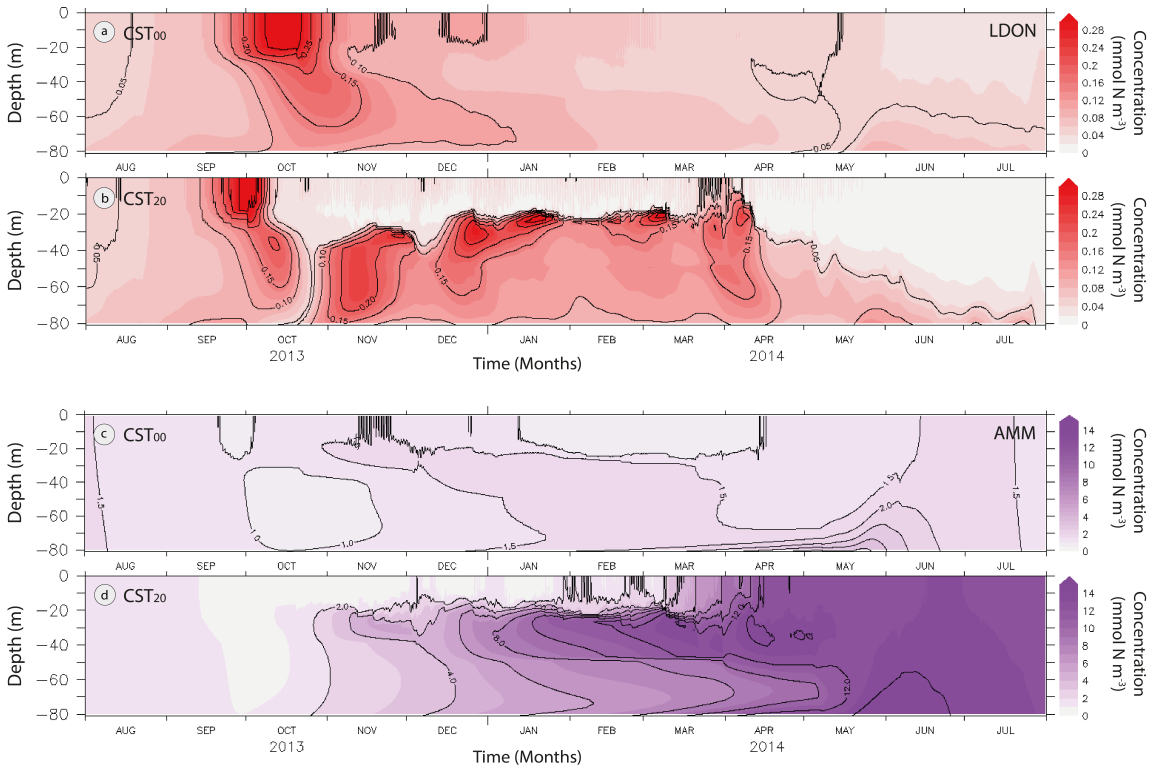

Figure 9. 2013/2014 annual cycle of simulated LDON from the **(a) CST$_{00}$** and the **(b) CST$_{20}$** simulations. 2013/2014 annual cycle of simulated ammonium from the **(c) CST$_{00}$** and the **(d) CST$_{20}$** simulations.

cycling of detritus below the thermocline. While detritus and LDON dynamics in the presence of HC were not found in literature, it is crucial to mention that biodegradation regulation is clearly not limited to one form of nutrient (Atlas and Bartha, 1972; Atlas, 1981; Shiller and Joung, 2012). Thus, understanding the preference and timing of the nitrogen-based nutrient consumption remains challenging.

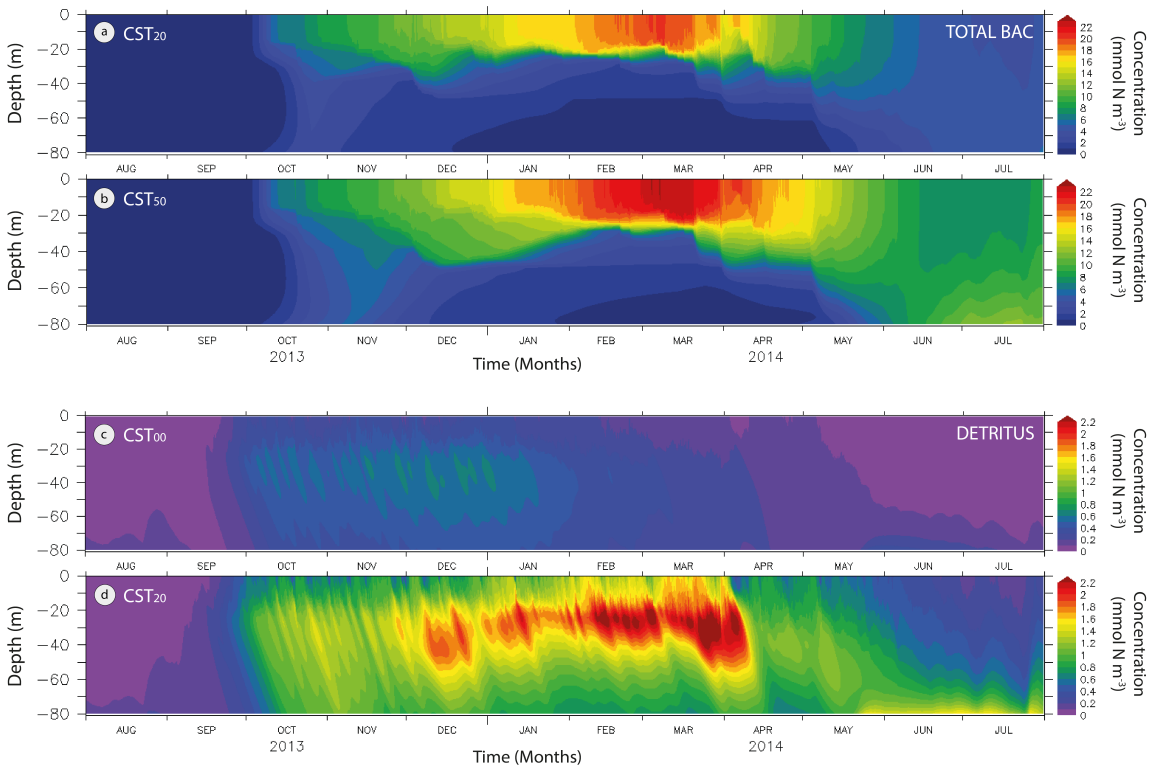

Figure 10. 2013/2014 annual cycle of simulated total bacteria (BAC1+BAC2) from **(a)** $\mathbf{CST}_{20}$ and **(b)** $\mathbf{CST}_{50}$ simulations and simulated detritus from **(c)** $\mathbf{CST}_{00}$ and **(d)** $\mathbf{CST}_{20}$ simulations.

1.4.4 Effects of HC on planktonic compartments

The planktonic response to HC was studied for the phytoplankton, zooplankton and the bacterial compartments. In figure 12 and 13, we chose to compare results from simulations at 20 mmol N m^{-3} of contamination to the control simulations.

First, in the stratified experiment, phytoplankton shows very high concentrations at all levels of contamination. Results from the $\mathbf{CST}_{20}$ simulation show maxima up to 8.7 times higher than the control values between 0 and 30 meters (Figure 12b). During the

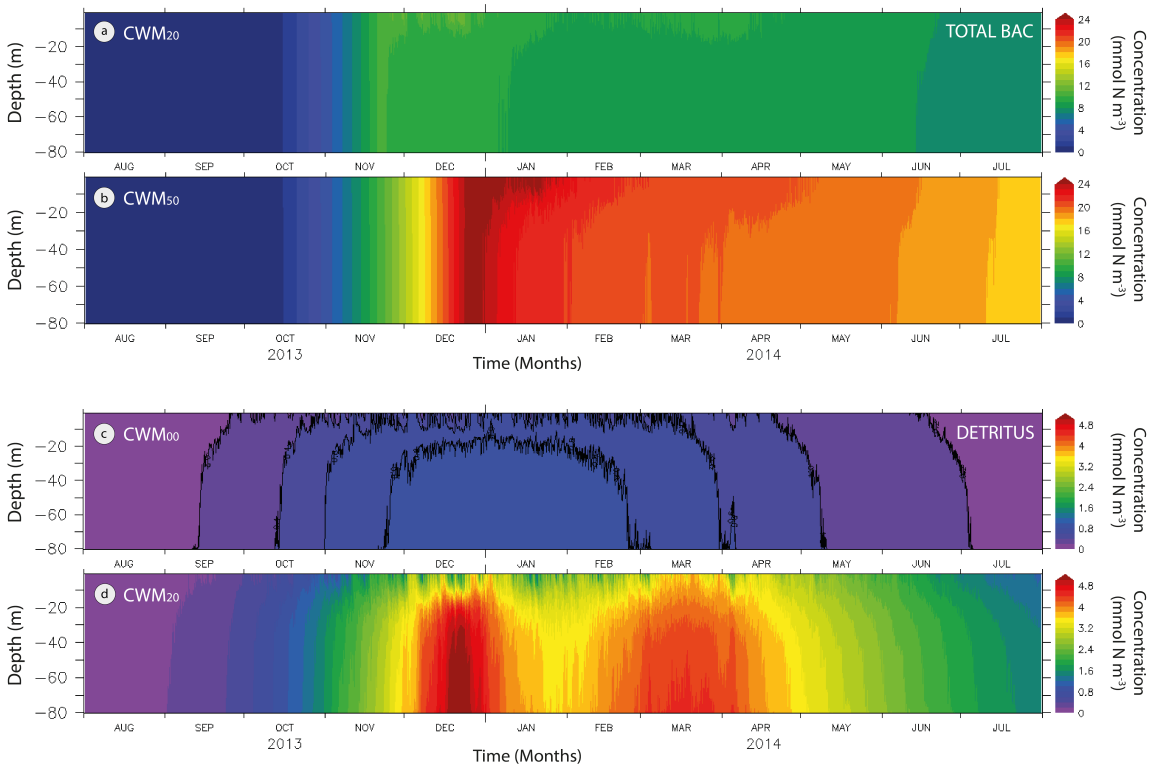

Figure 11. 2013/2014 annual cycle of simulated total bacteria (BAC1+BAC2) from **(a) CWM$_{20}$** and **(b) CWM$_{50}$** simulations and simulated detritus from **(c) CWM$_{00}$** and **(d) CWM$_{20}$** simulations.

first week of March 2014, converted chlorophyll-*a* values reach maxima up to 17.3 mg Chl-*a* m^{-3}. Moreover, a shift of the bloom periods from September (1.2 mmol N m^{-3}) and December 2013 (1.5 mmol N m^{-3}) to February (11.4 mmol N m^{-3}) and March 2014 (13 mmol N m^{-3}). This trend, detailed in section 1.4.5 is confirmed by high consumption of ammonium in the euphotic zone (Figure 9d) until the start of autumn.

However, the intensity of phytoplankton growth after HC contamination presented in this simulation has to be interpreted in relation with the effect of HC on the rest of the compartments and their indirect effect on phytoplankton growth. As observed in the

Baltic Sea during during the Tsesis oil spill (Johansson et al., 1980), in our simulations, at 20 mmol N m^{-3} of contamination, zooplankton is absent from the upper column until the third week of March 2014, therefore limiting grazing on phytoplankton and allowing its accumulation (Figure 12d).

Under the thermocline, the absence of HC makes it possible for zooplankton to grow and graze on sinking phytoplankton at the density interface. At 30 to 60 m depths, microzooplankton is dominant, feeding on bacterioplankton (Figure 12f). Compared to the control (Figure 12e), higher concentrations of BAC1 are only present below 30 m and highlight a stronger bacterial activity related to detritus recycling and sinking (Figure 12b and Figure 10d). This shift in the bacterial community structure in the upper water column in the $\mathbf{CST}_{20}$ simulation (Figure 10a) is in accordance with the diminution of bacterial diversity and a succession of γ-Proteobacteria, observed during the DWHs by Hazen et al. (2010) and Dubinsky et al. (2013).

In comparison, the well-mixed experiment results showed a relatively homogeneous vertical distribution of each variable presented in figure 13, as shown by Flores-Melo et al. (forthcoming). At the beginning of summer, concentrations of phytoplankton are not exceeding 1.5 and 4 mmol N m^{-3} for the $\mathbf{CWM}_{00}$ and $\mathbf{CWM}_{20}$ simulations, respectively. With a fast depletion of HC induced by biodegradation during the $\mathbf{CWM}_{20}$ simulation (Figure 7e), zooplankton starts to grow from the first week of December 2013 (Figure 13d). Here, lower concentrations of HC induced by strong vertical mixing reduce the impact on zooplankton (Figure 7e). Therefore, after the spring bloom period, zooplankton concentrations over 1.0 mmol N m^{-3} apply a grazing pressure limiting phytoplankton growth to 2 mmol N m^{-3} in January 2014.

Total bacterioplankton (Figure 11a), dominated by oil-degrading bacteria (80%) over

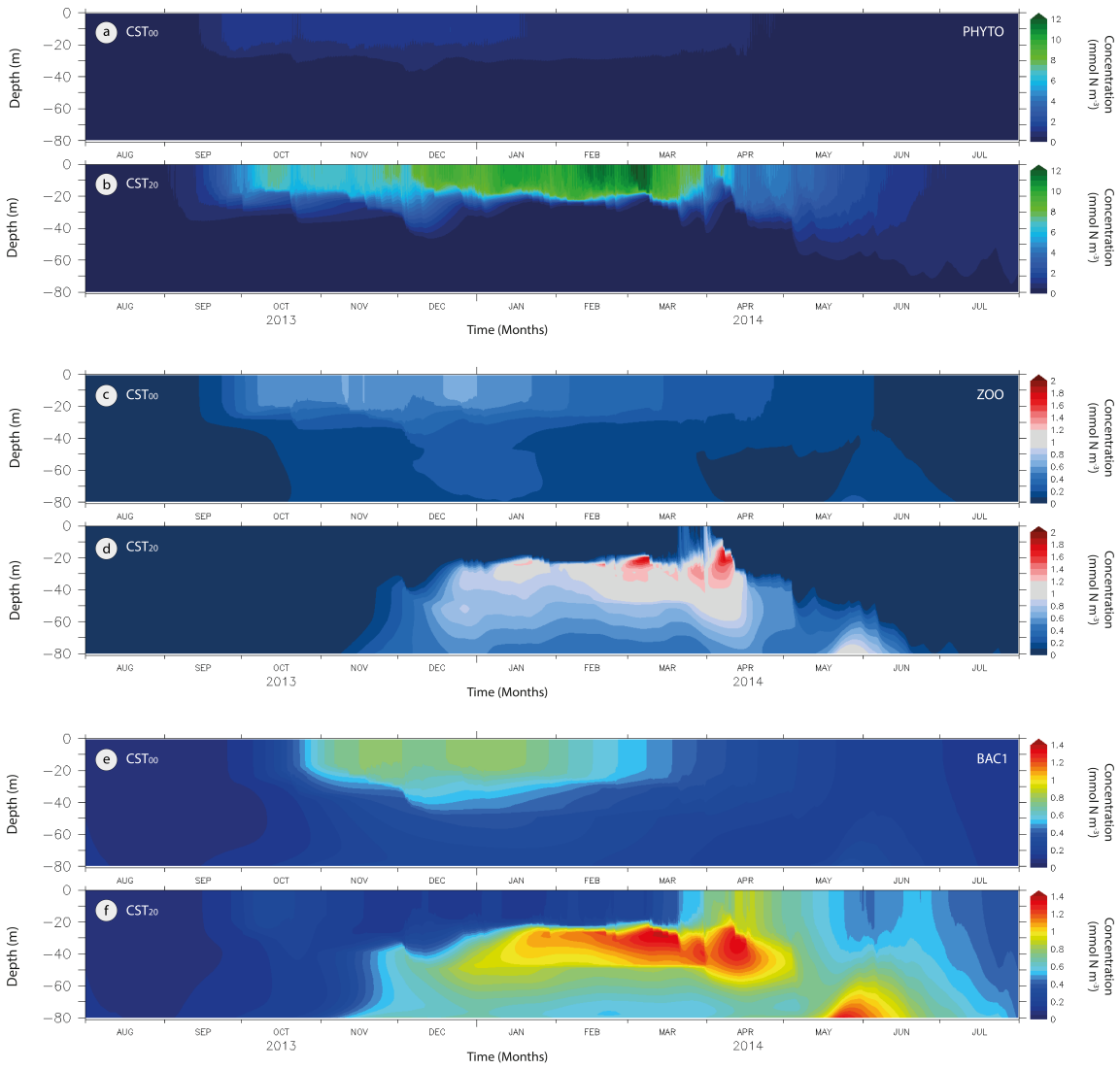

Figure 12. 2013/2014 annual cycle of simulated phytoplankton (DIA+FLA) from **(a)** $\mathbf{CST}_{00}$ and **(b)** $\mathbf{CST}_{20}$ simulations, simulated zooplankton (MCZ+MSZ) from **(c)** $\mathbf{CST}_{00}$ and **(d)** $\mathbf{CST}_{20}$ simulations and simulated bacteria (BAC1) from **(e)** $\mathbf{CST}_{00}$ and **(f)** $\mathbf{CST}_{20}$ simulations.

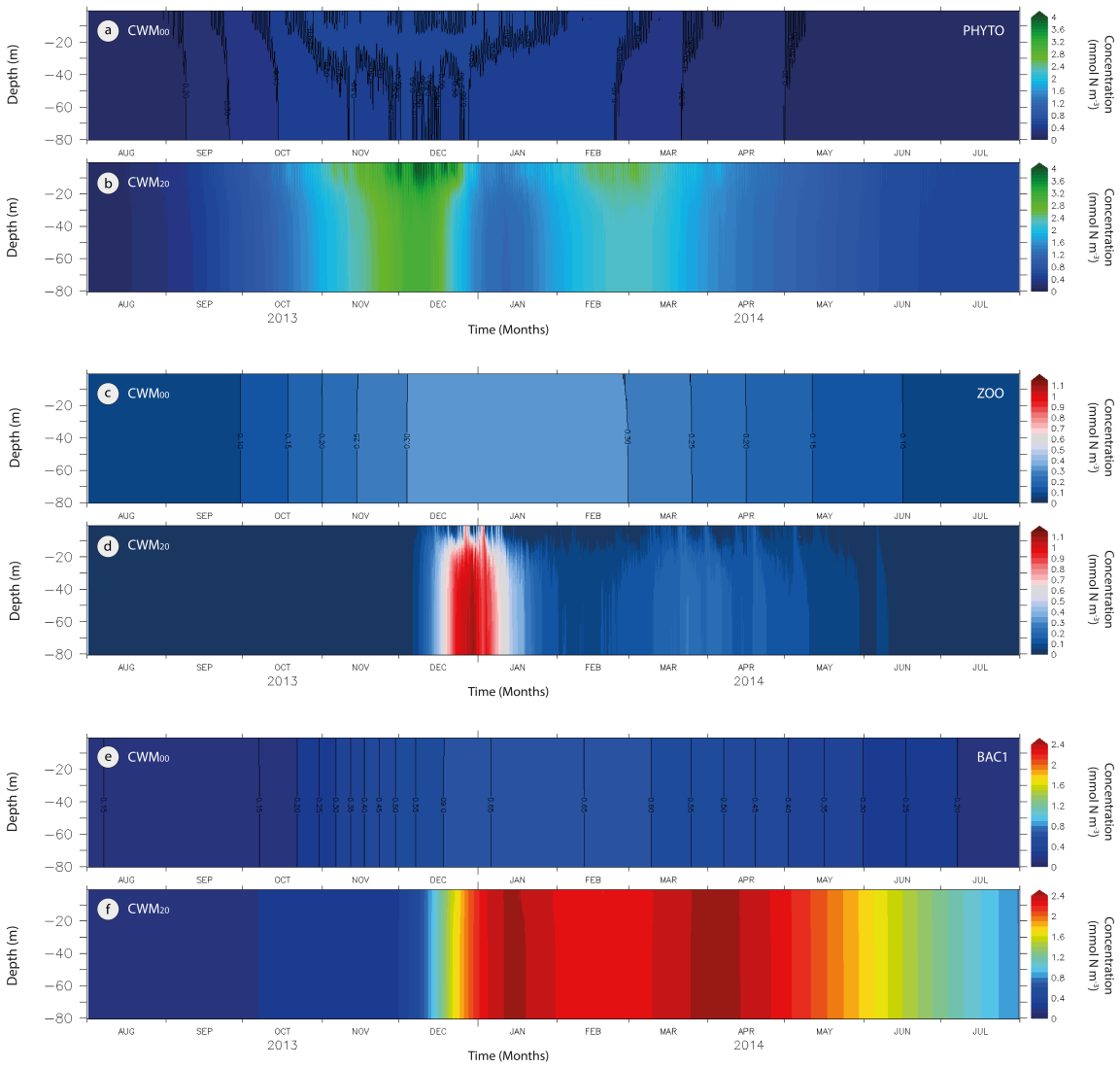

Figure 13. 2013/2014 annual cycle of simulated phytoplankton (DIA+FLA) from **(a)** $\mathbf{CWM_{00}}$ and **(b)** $\mathbf{CWM_{20}}$ simulations, simulated zooplankton (MCZ+MSZ) from **(c)** $\mathbf{CWM_{00}}$ and **(d)** $\mathbf{CWM_{20}}$ simulations and simulated bacteria (BAC1) from **(e)** $\mathbf{CWM_{00}}$ and **(f)** $\mathbf{CWM_{20}}$ simulations.

the entire **CWM**$_{20}$ simulation show concentrations (up to 24 mmol N m^{-3}) in the same range of the **CST**$_{20}$ results values (up to 22 mmol N m^{-3})(Figure 11b). However, after December 2013, BAC1 increases up to 4 times the control concentrations (Figure 13f) and therefore confirms the active sinking and transformation of exudation and mortality products to the detritus (Figure 11d) and LDON compartment (see section 1.4.3).

Results from **CST**$_{20}$ and **CWM**$_{20}$ show that bacterioplankton (BAC1 and BAC2) concentrations start increasing at the beginning of October 2013 (Figure 10b and 11b). This trend, following the increase of primary production, is clearly showing that low LDON concentrations are limiting bacterial increase during winter.

In the stratified experiment, biodegradation of HC is limited by LDON concentrations below 0.1 mmol N m^{-3} (Figure 9b) and HC concentrations spread to the bottom because of the absence of stratification. In the well-mixed experiment (results not shown), LDON concentrations below 0.12 mmol N m^{-3} are also delaying biodegradation until mid-October 2013.

Moreover, our results suggest that the physical regime plays an important role in biodegradation efficiency during a HC contamination. In the stratified experiment, most of the HC concentrations are removed by biodegradation by the first week of February 2014 (Figure 7b). In comparison, the well-mixed experiment shows a faster incorporation of HC by OHC Bacteria leading to the reduction of direct and indirect effects on plankton communities (Figure 13b and 13d). Here, although both HC and the concentration of bacteria are diluted over the entire water column, biodegradation of HC occurs more quickly than in the stratified experiment, where both compartments are confined to the upper water column. This is why zooplankton is less affected in the well-mixed than in the stratified experiment, and why these organisms prevent phytoplankton accumulation.

1.4.5 Temporal changes in planktonic size classes

To illustrate temporal dynamics, phytoplankton and zooplankton concentrations resulting from the **CST**$_{00}$, **CST**$_{10}$, **CST**$_{20}$ and **CST**$_{50}$ simulations were depth-integrated. In addition, since phytoplankton blooms are typically found in stratified two-layers conditions we will concentrate the interpretation of the stratified experiment only. Attention must be paid to the scale of figure 14a graphics, reduced from 280 to 50 mmol N m^{-2} for reading purposes.

Without HC in the system, diatoms are the dominant phytoplankton group with a spring bloom occurring in late September, as previously reported in the study area (Akselman and Carreto, 1996; Rivas et al., 2006). During the bloom peak, both micro- and mesozooplankton concentrations start to increase in our model through herbivorous grazing, thus limiting diatoms' growth. Unfortunately, no field information is available to validate our results.

In **CST**$_{10}$ (Figure 14b) the diatom bloom reaches 5 times the values found for the **CST**$_{00}$ simulation and persists until the end of November. Two weaker diatom blooms can be noted on the third week of January 2014 and the third week of March 2014. Both are followed by mesozooplankton growth issued from grazing. At this level of perturbation, microzooplankton shows an interesting evolution. From the end of August 2013, its concentration increases despite the presence of HC in seawater. These results can be linked to microzooplankton grazing on bacterioplankton occurring in the lower part of the water column where HC concentrations $\leq$ 1 mmol N m^{-3} (Figure 7a).

Simulations **CST**$_{20}$ and **CST**$_{50}$ results show a strong dominance of diatom biomass over the other compartments. Micro- and mesozooplankton concentrations increase from the first week of November 2013, both with a similar trend (Figure 14c and 14d).

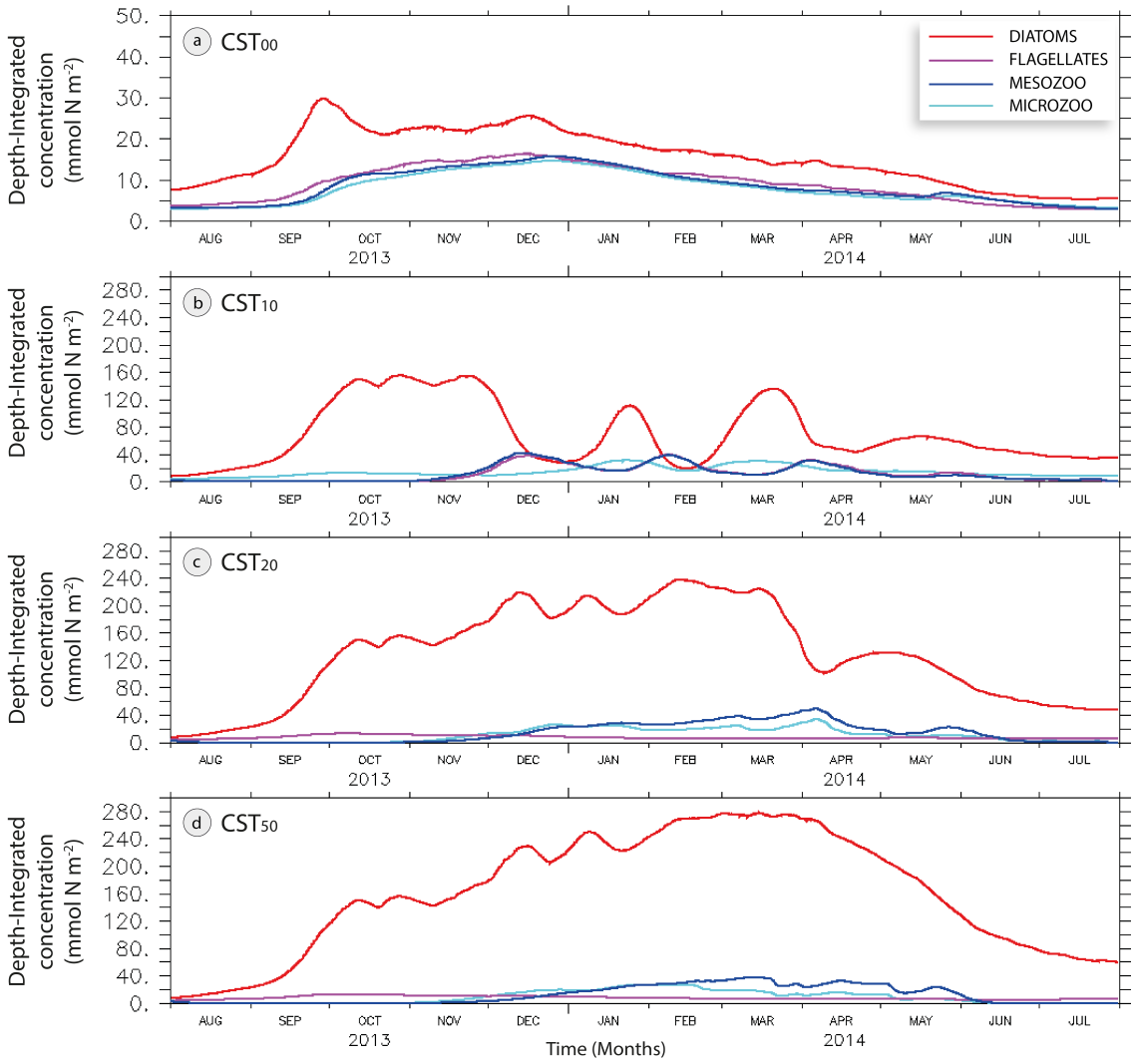

Figure 14. 2013/2014 annual cycle of Simulated Depth-integrated Diatoms (red curve), Flagellates (purple curve), microzooplankton (cyan curve) and mesozooplankton (blue curve) at **(a)** 0 mmol N m^{-3}, **(b)** 10 mmol N m^{-3} **(c)** 20 mmol N m^{-3} and **(d)** 50 mmol N m^{-3} of contamination for the Stratified Experiment.

While our results show high diatoms' growth linked to indirect effects of HC contamination, results from other works are controversial: some studies show strong neg-

ative effects on this group (Hsiao, 1976; Siron et al., 1996; Nayar et al., 2005; Sargian et al., 2007) and others highlight diatom growth in oil polluted environments (Gordon and Prouse, 1973; Johansson et al., 1980; Teal and Howarth, 1984). Here we show that among the indirect effects, the decrease of zooplankton grazing leads to an increase in phytoplankton, as shown by Johansson et al. (1980). Similarly, the increase of bacterial activity associated with the recycling of dead organisms was previously observed by Baker (1971) and Cabioch et al. (1981). The previous results indicate that the response of phytoplankton to HC contamination is species-specific. Therefore, investigation is needed to carefully parameterize direct effects on phytoplankton.

1.5 Conclusions

Modelling the effects of HC on a planktonic system implies considering several biogeochemical variables and processes that will result in a direct imbalance of carbon fluxes occurring in natural pelagic systems over an annual cycle. However, our results suggest that other than the direct effects, indirect effects have to be taken into consideration.

The highly productive south-eastern portion of the SJG shows different trends after a subsurface incorporation of HC. In both experiments, at 10, 20 and 50 mmol N m^{-3} of contamination, biodegradation of HC is limited during winter and starts at the beginning of spring only when primary production increases and, consequently, when LDON concentrations are high enough.

At 20 mmol N m^{-3}, abnormally elevated concentrations of ammonium are linked to strong recycling of detritus by bacteria (BAC1). In this case, the detritus compartment is fuelled by dead zooplankon related to HC toxicity and strong phytoplankton exudation. Because the nitrification process is not taken into consideration, the incorporation of HC

in the planktonic system is reflected in the accumulation of nitrogen in the ammonium compartment.

A large dominance of diatoms over the other planktonic compartments is associated with the above-mentioned indirect effects (decrease of herbivorous grazing and increase of detritus formation).

Finally, the dynamically contrasting well-mixed region shows lower HC concentrations over the entire water column resulting in a faster bacterial consumption. Nevertheless, with the combination of lower HC concentrations and a more effective biodegradation, zooplankton is less affected by contamination in these physical conditions.

In future works, several key parameterizations should help us refine the results presented in this study. First, sensitivity analyzes must be conducted to understand the importance of biodegradation rates and nutrient dependency on biodegradation. Then, given the intensity of phytoplankton growth in relation with the reduction of grazing, direct effects of HC on phytoplankton and particularly on diatoms must be considered at both, species-specific levels, and for different HC concentrations, which have been shown to either stimulate or prevent diatoms' growth.

CONCLUSION GÉNÉRALE

L'étude numérique de l'effet des hydrocarbures sur le système planctonique côtier du GSJ a été réalisée à partir d'un modèle physique couplé à un modèle biogéochimique. Ce couplage a permis de considérer l'influence du régime hydrodynamique vertical sur les flux biogéochimiques intervenant lors d'une pollution par les hydrocarbures. Un scénario de contamination chronique, incluant plusieurs niveaux de perturbation, a été choisi pour mettre en évidence l'importance des processus et variables jouant un rôle direct et indirect dans la modification des flux de carbone présents dans l'écosystème pélagique durant ce type d'évènement.

Dans les deux expériences de contamination, le démarrage de la biodégradation des hydrocarbures et la croissance des bactéries "OHCB" semble être synchronisé avec le début de la période productive de l'été austral. Cette particularité a également pu être observée pour des simulations (non présentées) dans lesquelles la contamination a débuté à d'autres périodes de l'année. Ce phénomène est associée à la limitation de la croissance des bactéries (BAC1 et BAC2) par de faibles consomations en LDON.

En comparaison, la zone bien mélangée présente des concentrations en HC plus faibles sur la totalité de la colonne d'eau et implique par conséquent une consommation bactérienne plus rapide du contaminant. Les communautés zooplanctoniques semblent être moins affectées à des niveaux de contamination équivalents. Dans le cas de ces simulations, un régime hydrodynamique engendrant des conditions homogènes explique ces résultats.

Le compartiment des diatomées présente une forte dominance sur le reste des autres compartiments planctoniques. Cet effet indirect important est associé aux effets directs des

hydrocarbures sur le zooplancton. En effet, l'importante mortalité du micro- et mésozooplancton entraine une réduction du broutage dans la zone euphotique et favorise la formation de détritus.

Des concentrations élevées en ammonium observées dans les deux expériences contaminées témoignent d'un recyclage important du compartiment détritique par les bactéries (BAC1). L'augmentation de la concentration en detritus est associée à la forte mortalité du zooplancton par toxicité aux HC mais aussi par l'exudation du phytoplancton présent en grande quantité.

Cette étude constitue une avancée dans la compréhension des interactions entre certains groupes planctoniques et la dynamique des hydrocarbures lors d'un évènement de pollution chronique. Cependant, des travaux supplémentaires peuvent être menés dans le but de paramétriser de manière précise les effets sur le plancton. Premièrement, une série d'analyses de sensibilité doivent être menées dans le but de comprendre l'importance des taux de biodégradation des HC et leur dépendance aux nutriments. Ensuite, compte tenu de l'augmentation de la concentration phytoplanctonique associée à la diminution du broutage, il est nécessaire de considérer les effets directs des HC sur la croissance et la mortalité du phytoplancton et particulierèrement des diatomées. Ces effets directs doivent être pris en compte à la fois pour des espèces spécifiques mais aussi pour différentes concentrations en HC.

De plus, une série d'expériences en mésocosmes, incluant une communauté bactérienne et phytoplanctonique spécifique de la région étudiée, serait considérée comme un bon outil complémentaire pour quantifier la réponse du phytoplancton a une contamination par les HC. De plus, certains mésocosmes permettent de simuler des conditions de mélange différentes, incluant ainsi une variable physique dans l'évolution de ces processus biolo-

giques.

Alors que ces modèles restent à améliorer dans le but de mieux comprendre l'évolution temporelle de la réponse planctonique à ce type de perturbation, ils constituent une étape essentielle dans le cheminement vers des modèles plus complexes en 3 dimensions.

ANNEXE I

BIOGEOCHEMICAL PARAMETERS

The table below summarizes the GOTM names, reference symbols, values used for the simulations, units and definitions of the biogeochemical parameters in the model.

GOTM	Symbol	Value	Unit	Definition	Reference
p1initial	C_1^{init}	0.05	mmol N m^{-3}	Small phytoplankton initial concentration	(Tremblay et al., 2006)
p2initial	C_2^{init}	0.05	mmol N m^{-3}	Large phytoplankton initial concentration	(Tremblay et al., 2006)
z1initial	C_3^{init}	0.05	mmol N m^{-3}	Small zooplankton initial concentration	(Tremblay et al., 2006)
z2initial	C_4^{init}	0.05	mmol N m^{-3}	Large zooplankton initial concentration	(Tremblay et al., 2006)
binitial	C_5^{init}	0.00	mmol N m^{-3}	Traditional (BAC1) and OHC Bacteria (BAC2) initial concentration	-
dinitial	C_7^{init}	0.40	mmol N m^{-3}	Detritus initial concentration	(Harrison and Platt, 1986)
linitial	C_8^{init}	0.14	mmol N m^{-3}	LDON initial concentration	-
p0	C_1^{min}	0.00	mmol N m^{-3}	Minimal phytoplankton concentration	-
z0	C_3^{min}	0.00	mmol N m^{-3}	Minimal zooplankton concentration	-
b0	C_5^{min}	0.00	mmol N m^{-3}	Minimal bacteria concentration	-
vp1	vp_1	1.50	day^{-1}	Maximal uptake rate of small phytoplankton	-
alpha1	a_1	0.07	m^{-2} W^{-1} day^{-1}	Slope of the small phytoplankton PI-curve	-
inib1	b_1	0.05	m^{-2} W^{-1} day^{-1}	Inhibition slope of the small phytoplankton	-
vp2	vp_2	1.50	day^{-1}	Maximal uptake rate of large phytoplankton	-
alpha2	a_2	0.07	m^{-2} W^{-1} day^{-1}	Slope of the large phytoplankton PI-curve	-
inib2	b_2	0.05	m^{-2} W^{-1} day^{-1}	Inhibition slope of the large phytoplankton	-
theta	Θ	0.00	day	Phytoplankton buoyancy parameter	-
wp1min	wp_1^{min}	-0.06	m day^{-1}	Minimal small phytoplankton settling velocity	-
wp1max	wp_1^{max}	-0.38	m day^{-1}	Maximal small phytoplankton settling velocity	-
wp2min	wp_2^{min}	-0.06	m day^{-1}	Minimal large phytoplankton settling velocity	-
wp2max	wp_2^{max}	-0.38	m day^{-1}	Maximal large phytoplankton settling velocity	-
kn1	Kn_1	0.20	mmol N m^{-3}	Half saturation constant of nitrate uptake by small phytoplankton	-
ka1	Ka_1	0.80	mmol N m^{-3}	Half saturation constant of ammonium uptake by small phytoplankton	-
kn2	Kn_2	0.20	mmol N m^{-3}	Half saturation constant of nitrate uptake by large phytoplankton	-
ka2	Ka_2	0.80	mmol N m^{-3}	Half saturation constant of ammonium uptake by large phytoplankton	(Lima et al., 2002)
mu11	μ_{11}	0.05	day^{-1}	Mortality rate of small phytoplankton	(Lima et al., 2002)
mu12	μ_{12}	0.05	day^{-1}	Mortality rate of large phytoplankton	-
k5	K_5	0.20	mmol N m^{-3}	Half saturation constant of ingestion	-
gamma	γ	0.05	-	Exudation fraction	-
wp1	wp_1	-0.50	m day^{-1}	Small phytoplankton settling velocity	-
wp2	wp_2	-0.50	m day^{-1}	Large phytoplankton settling velocity	-
g1max	g_1^{max}	1.00	day^{-1}	Maximal small zooplankton ingestion	-
g2max	g_2^{max}	1.00	day^{-1}	Maximal lalrge zooplankton ingestion	-

GOTM	Symbol	Value	Unit	Definition and Reference	-
k3	K_3	1.00	mmol N m^{-3}	Half saturation constant of ingestion	(Burchard et al., 2006)
beta	β	0.625	-	Grazing efficiency	(Burchard et al., 2006)
mu21	μ_{21}	0.30	day^{-1}	Mortality rate of small zooplankton	-
mu21max	μ_{21}^{max}	1.50	day^{-1}	Maximal Mortality rate of small zooplankton from hydrocarbon toxicity	-
mu21hc	μ_{21}^{HC}	eq.(8.1)	day^{-1}	Mortality rate of small zooplankton from hydrocarbon toxicity	-
k6	K_6	0.60	mmol N m^{-3}	Half saturation constant of zooplankton loss (small and large)	-
k6hc	K_6^{HC}	31.4	mmol N m^{-3}	Half saturation constant of small and large zooplankton loss by HC toxicity	-
mu22	μ_{22}	0.30	day^{-1}	Mortality rate of large zooplankton	-
mu22max	μ_{22}^{max}	1.50	day^{-1}	Maximal Mortality rate of large zooplankton from hydrocarbon toxicity	-
mu22hc	μ_{22}^{HC}	eq.(8.1)	day^{-1}	Mortality rate of large zooplankton from hydrocarbon toxicity	-
delta	δ	0.10	-	Fractional zooplantkon loss of LDON	(Burchard et al., 2006)
epsi	ϵ	0.70	-	Fractional zooplankton loss of ammonium	(Burchard et al., 2006)
r11	r_{11}	0.55	-	Small zooplankton preference on small phytoplankton	-
r12	r_{12}	0.30	-	Small zooplankton preference on large phytoplankton	-
r13	r_{13}	0.05	-	Small zooplankton preference on Traditional and OHC Bacteria	-
r14	r_{14}	0.10	-	Small zooplankton preference on detritus	-
r21	r_{21}	0.50	-	Large zooplankton preference on small phytoplankton	-
r22	r_{22}	0.30	-	Large zooplankton preference on large phytoplankton	-
r23	r_{23}	0.05	-	Large zooplankton preference on detritus	-
r24	r_{24}	0.15	-	Large zooplankton preference on small zooplankton	-
vb1	vb_1	1.20	day^{-1}	Maximal uptake rate of large Traditional bacteria	(Burchard et al., 2006)
vb2	vb_2	1.20	day^{-1}	Maximal uptake rate of large OHC bacteria	(Burchard et al., 2006)
k4	K_4	0.50	mmol N m^{-3}	Half saturation constant of Traditional bacteria uptake	-
k10	K_{10}	0.15	mmol N m^{-3}	Half saturation constant of OHC bacteria uptake	-
wh	wh	0.00	m day^{-1}	Hydrocarbon settling velocity	-
mu3	$\mu 3$	0.15	day^{-1}	Bacterial excretion rate	-
etaa	η_a	0.00	m day^{-1}	Uptake ratio Ammonium : LDON	-
etah	η_h	0.00	m day^{-1}	Uptake ratio Hydrocarbon : LDON	-
mu4	μ_4	0.02	day^{-1}	Detritus breakdown rate	-
mu5	μ_5	0.00	day^{-1}	Nitrification rate	-
wd	wh	-2.00	m day^{-1}	Detritus settling velocity	-
kc	Kc	0.03	m^2 mmol N $^{-1}$	Attenuation constant for self shading	-

ANNEXE II

BIOGEOCHEMICAL EQUATIONS

Symbol	Variable
C_1	Flagellates
C_2	Diatoms
C_3	Microzooplankton
C_4	Mesozooplankton
C_5	Bacteria (Traditional)
C_6	Bacteria (Obligate Hydrocarbon Degrading Bacteria)
C_7	Detritus
C_8	Nitrate
C_9	Lablile Dissolved Organic Nitrogen (LDON)
C_{10}	Ammonium
C_{11}	Dissolved Hydrocarbon

References of the 11 concentrations symbols and definitions for the biogeochemical model

Lecture note : $C_{o,i}$ with $o \Rightarrow$ output concentration and $i \Rightarrow$ input concentration

B.1 Phytoplankton nutrient uptake

Nitrate uptake by flagellates

$$C_{8,1} = ff_1 \; Qn_1 \; (C_1 + C_1^{min}) \tag{B.1.1}$$

Ammonium uptake by flagellates

$$C_{10,1} = ff_1 \; Qa_1 \; (C_1 + C_1^{min}) \tag{B.1.2}$$

Nitrate uptake by diatoms

$$C_{8,2} = ff_2 \; Qn_2 \; (C_2 + C_1^{min}) \tag{B.1.3}$$

Ammonium uptake by diatoms

$$C_{10,2} = ff_2 \; Qa_2 \; (C_2 + C_1^{min}) \tag{B.1.4}$$

Light inhibition factor for flagellates

$$ff_1 = ps_1 \; (1 - e^{-\alpha_1 \frac{PAR(ci)}{ps_1}}) \; e^{-1 \frac{(inib_1 \; PAR(ci))}{ps_1}} \tag{B.1.5}$$

Photosystem function for flagellates' light inhibition

$$ps_1 = \frac{vp_1}{(\frac{\alpha_1}{\alpha_1 + inib_1})} (\frac{\alpha_1}{\alpha_1 + inib_1})^{\frac{inib_1}{\alpha_1}} \tag{B.1.6}$$

Light inhibition factor for diatoms

$$ff_2 = ps_2 \, (1 - e^{-\alpha_2 \frac{PAR(ci)}{ps_2}}) \, e^{-1 \frac{(inib_1 \, PAR(ci))}{ps_2}} \tag{B.1.7}$$

Photosystem function for diatoms' light inhibition

$$ps_2 = \frac{vp_2}{(\frac{\alpha_2}{\alpha_2 + inib_2})} (\frac{\alpha_2}{\alpha_2 + inib_2})^{\frac{inib_2}{\alpha_2}} \tag{B.1.8}$$

Nitrate limitation factor for flagellates growth

$$Qn_1 = \frac{\frac{C_8}{Kn_1}}{\frac{1 + C_8}{\frac{(Kn_1 + C_{10})}{Ka_1}}} \tag{B.1.9}$$

Ammonium limitation factor for flagellates growth

$$Qa_1 = \frac{\frac{C_{10}}{Ka_1}}{\frac{1 + C_8}{\frac{(Kn_1 + C_{10})}{Ka_1}}} \tag{B.1.10}$$

Nitrate limitation factor for diatoms growth

$$Qn_2 = \frac{\frac{C_8}{Kn_2}}{\frac{1 + C_8}{\frac{(Kn_1 + C_{10})}{Ka_2}}} \tag{B.1.11}$$

Ammonium limitation factor for diatoms growth

$$Qa_2 = \frac{\frac{C_{10}}{Ka_2}}{\frac{1 + C_8}{\frac{(Kn_1 + C_{10})}{Ka_2}}} \tag{B.1.12}$$

B.2 Grazing and uptake by zooplankton

Flagellates mortality and grazing by microzooplankton

$$C_{1,3} = \beta \, g_1^{max} \, r_{11} \, {C_1}^2 \, Fac_1 \tag{B.2.1}$$

Diatoms mortality and grazing by nicrozooplankton

$$C_{2,3} = \beta \, g_1^{max} \, r_{12} \, {C_2}^2 \, Fac_1 \tag{B.2.2}$$

Grazing of OHC Bacteria by microzooplankton

$$C_{5,3} = \beta\, g_1^{max}\ \frac{1}{2}\, r_{13}\, C_5{}^2\, Fac_1 \qquad \text{(B.2.3)}$$

Grazing of OHC Bacteria by microzooplankton

$$C_{6,3} = \beta\, g_1^{max}\ \frac{1}{2}\, r_{13}\, C_6{}^2\, Fac_1 \qquad \text{(B.2.4)}$$

Grazing of detritus by microozooplankton

$$C_{7,3} = \beta\, g_1^{max}\, r_{14}\, C_7{}^2\, Fac_1 \qquad \text{(B.2.5)}$$

Microzooplankton preference normalization factor

$$Fac_1 = \left(\frac{C_3 + C_3^{min}}{K_3(r_{11}\, C_1)}+(r_{12}\, C_2)+\left(\frac{1}{2}\, r_{13}\, C_6\right)+(r_{14}\, C_7)+(r_{11}\, C_1)^2+(r_{12}\, C_2)^2+\frac{1}{2}\, r_{13}\, (C_5+C_6)^2+(r_{14}\, C_7^2)\right) \qquad \text{(B.2.6)}$$

Flagellates mortality and grazing by mesozooplankton

$$C_{1,4} = \beta\, g_2^{max}\, r_{21}\, C_1{}^2\, Fac_2 \qquad \text{(B.2.7)}$$

Diatoms mortality and grazing by mesozooplankton

$$C_{2,4} = \beta\, g_2^{max}\, r_{22}\, C_2{}^2\, Fac_2 \qquad \text{(B.2.8)}$$

Grazing of detritus by mesozooplankton

$$C_{7,4} = \beta\ g_1^{max}\ r_{23}\ {C_7}^2\ Fac_2 \tag{B.2.9}$$

Grazing of microzooplankton by mesozooplankton

$$C_{3,4} = \beta\ g_1^{max}\ r_{24}\ {C_3}^2\ Fac_2 \tag{B.2.10}$$

Mesozooplankton preference normalization factor

$$Fac_2 = \frac{C_4 + C_3^{min}}{K_3\ (r_{21}\ C_1)} + (r_{22}\ C_2) + (\frac{1}{2}\ r_{23}\ C_7) + (r_{24}\ C_3) + (r_{21}\ C_1)^2 + (r_{22}\ C_2)^2 + (\frac{1}{2} r_{23} C_7^2) + (r_{24}\ C_3^2) \tag{B.2.11}$$

B.3 Zooplankton mortality and exsudation

Degradation of microzooplankton in detritus

$$C_{3,7} = (1 - \beta_z)\ (g_2^{max}\ r_{24}\ {C_6}^2\ Fac_2) + (1 - \epsilon - \delta)\ \mu_{21}^{HC}\ \frac{(C_3 + C_3^{min})}{K_6 + (C_3 + C_3^{min})}\ C_3 \tag{B.3.1}$$

Degradation of mesozooplankton in detritus

$$C_{4,7} = (1 - \epsilon - \delta)\ \mu_{22}^{HC}\ \frac{(C_4 + C_3^{min})}{K_6 + (C_4 + C_3^{min})}\ C_4 \tag{B.3.2}$$

Microzooplankton mortality rate

$$\mu_{21}^{HC} = \mu_{21} + (\mu_{21}^{max} - \mu_{21}) \left(\frac{(C_{11})^5 + (C_{11}^{min})^5}{(K_6^{HC})^5} \right) \tag{B.3.3}$$

Mesozooplankton mortality rate

$$\mu_{22}^{HC} = \mu_{21}^{HC} \tag{B.3.4}$$

Exsudation of microzooplankton in ammonium

$$C_{3,10} = \epsilon \, \mu_{21}^{HC} \, \frac{(C_3 + C_3^{min})}{K_6 + (C_3 + C_3^{min})} \, C_3 \tag{B.3.5}$$

Exsudation of microzooplankton in Labile Dissolved Organic Nitrogen

$$C_{3,9} = \delta \, \mu_{21}^{HC} \, \frac{(C_3 + C_3^{min})}{K_6 + (C_3 + C_3^{min})} \, C_3 \tag{B.3.6}$$

Exsudation of mesozooplankton in ammonium

$$C_{4,10} = \epsilon \, \mu_{22}^{HC} \, \frac{(C_4 + C_3^{min})}{K_6 + (C_4 + C_3^{min})} \, C_4 \tag{B.3.7}$$

Exsudation of mesozooplankton in Labile Dissolved Organic Nitrogen

$$C_{4,9} = \delta \, \mu_{22}^{HC} \, \frac{(C_4 + C_3^{min})}{K_6 + (C_4 + C_3^{min})} \, C_4 \tag{B.3.8}$$

B.4 Phytoplankton mortality and exsudation

Exudation of flagellates to labile dissolved organic nitrogen

$$C_{1,10} = \gamma \; P(E) \; \frac{\frac{C_8}{Kn_1} + \frac{C_9}{Ka_1}}{\frac{C_8}{Kn_1} + \frac{C_9}{Ka_1}} \; C_1 \tag{B.4.1}$$

Exudation of diatoms to labile dissolved organic nitrogen

$$C_{2,10} = \gamma \; P(E) \; \frac{\frac{C_8}{Kn_2} + \frac{C_9}{Ka_2}}{\frac{C_8}{Kn_2} + \frac{C_9}{Ka_2}} \; C_2 \tag{B.4.2}$$

Mortality of flagellates to detritus

$$C_{1,7} = \frac{\mu_{11} \; (C_1 + C_1^{min})}{K_5 + C_1 + C_1^{min} \; C_1} + (1 - \beta) \; {C_1}^2 \; (g_1^{max} \; r_{11} \; Fac_1) + (\;) g_2^{max} \; r_{21} \; Fac_2) \tag{B.4.3}$$

Mortality of diatoms to detritus

$$C_{2,7} = \frac{\mu_{12} \; (C_2 + C_1^{min})}{K_5 + C_2 + C_1^{min} \; C_2} + (1 - \beta) \; {C_2}^2 \; (g_1^{max} \; r_{12} \; Fac_1) + (g_2^{max} \; r_{22} \; Fac_2) \tag{B.4.4}$$

B.5 Nutrient and hydrocarbon uptake by bacteria

Ammonium uptake by traditional bacteria

$$C_{10,5} = \frac{vb_1 \; min_{AL}}{k_4 + min_{AL} + C_9 \; (C_5 + C_5^{min})} \tag{B.5.1}$$

Labile Dissolved Organic Nitrogen uptake by traditional bacteria

$$C_{9,5} = \frac{vb_1 \; C_9}{k_4 + min_{AL} + C_9 \; (C_5 + C_5^{min})} \tag{B.5.2}$$

Hydrocarbon uptake by OHC bacteria

$$C_{11,6} = vb_2 \; min_{HL} \; (C_6 + C_5^{min}) \tag{B.5.3}$$

Labile Dissolved Organic Nitrogen uptake by OHC bacteria

$$C_{9,6} = vb_2 \; eta_h \; min_{HL} \; (C_6 + C_5^{min}) \tag{B.5.4}$$

B.6 Nutrient and hydrocarbon limitation factors

Minimal Ammonium to Labile Dissolved Organic Nitrogen uptake ratio for traditional bacteria

$$min_{AL} = min\ (C_{10}, \eta_a\ C_9) \tag{B.6.1}$$

Minimal HC to Labile Dissolved Organic Nitrogen uptake ratio for OHC bacteria

$$min_{HL} = min\ (\frac{C_{11}}{K_{10} + C_{11}},\ \frac{C_9}{K_4 + C_9}) \tag{B.6.2}$$

B.7 Other processes

Exsudation of traditional bacteria to detritus

$$C_{5,7} = \mu_3\ C_5 \tag{B.7.1}$$

Exsudation of Obligate HC bacteria to detritus

$$C_{6,7} = \mu_3\ C_6 \tag{B.7.2}$$

Breakdown of detritus into Labile Dissolved Organic Nitrogen

$$C_{7,9} = \mu_4\ C_3 \tag{B.7.3}$$

Nitrification

$$C_{10,8} = \mu_5 \, C_{10} \tag{B.7.4}$$

RÉFÉRENCES

Acha, E. M., Mianzan, H. W., Guerrero, R. A., Favero, M., Bava, J., 2004. Marine fronts at the continental shelves of austral South America: Physical and ecological processes. Journal of Marine Systems 44 (1-2), 83–105.

Akselman, R., Carreto, J. I., 1996. Estudios Ecologicos en el Golfo San Jorge y Adyacencias (Antlantico Sudoccidental). Distribucion, Abundencia y variacion estacional del fitoplancton en relacion a factores fisico-quimicos y la dinamica hidrologica). Ph.D. thesis, Universidad de Buenos Aires.

Almeda, R., Wambaugh, Z., Wang, Z., Hyatt, C., Liu, Z., Buskey, E. J., jan 2013. Interactions between zooplankton and crude oil: toxic effects and bioaccumulation of polycyclic aromatic hydrocarbons. PloS ONE 8 (6), e67212.

Anderson, J. W., Neff, J. M., Cox, B. a., Tatem, H. E., Hightower, G. M., 1974. Characteristics of dispersions and water-soluble extracts of crude and refined oils and their toxicity to estuarine crustaceans and fish. Marine Biology 27 (1), 75–88.

Atlas, R. M., 1981. Microbial degradation of petroleum hydrocarbons: an environmental perspective. Microbiology and Molecular Biology Reviews 45 (1), 180–209.

Atlas, R. M., Bartha, R., 1972. Degradation and mineralization of petroleum in sea water: limitation by nitrogen and phosphorous. Biotechnology and Bioengineering 14 (3), 309–318.

Baker, J. M., 1971. Seasonal Effects of Oil Pollution on Salt Marsh Vegetation. Oikos, Nordic Society 22 (1), 106–110.

Barata, C., Calbet, A., Saiz, E., Ortiz, L., Bayona, J. M., nov 2005. Predicting single and mixture toxicity of petrogenic polycyclic aromatic hydrocarbons to the copepod Oithona davisae. Environmental toxicology and chemistry / SETAC 24 (11), 2992–2999.

Beazley, M. J., Martinez, R. J., Rajan, S., Powell, J., Piceno, Y. M., Tom, L. M., Andersen, G. L., Hazen, T. C., van Nostrand, J. D., Zhou, J., Mortazavi, B., Sobecky, P. A., 2012. Microbial community analysis of a coastal salt marsh affected by the Deepwater Horizon oil spill. PLoS ONE 7 (7), e41305.

Bisbal, G. A., 1995. The Southeast South American shelf large marine ecosystem Evolution and components. Marine Policy 19 (1), 21–38.

Brown, C. E., Fieldhouse, B., Lumley, T. C., Lambert, P., Hollebone, B. P., 2011. Oil Spill Science and Technology, mervin fingas Edition. Gulf Professional Publishing/Elsevier.

Burchard, H., Bolding, K., Kühn, W., Meister, A., Neumann, T., Umlauf, L., jul 2006. Description of a flexible and extendable physical–biogeochemical model system for the water column. Journal of Marine Systems 61 (3-4), 180–211.

Cabioch, L., Dauvin, J., Gentil, F., Retière, C., Rivain, V., 1981. Perturbations induites dan la composition et le fonctionnement des peuplements benthiques sublittoraux, sous l'effet des hydrocarbures de l'Amoco Cadiz. Amoco Cadiz, fates and effects of the oil spill (CNEXO), 513–526.

Cappello, S., Denaro, R., Genovese, M., Giuliano, L., Yakimov, M. M., jan 2007. Predominant growth of Alcanivorax during experiments on "oil spill bioremediation" in mesocosms. Microbiological research 162 (2), 185–90.

Carbajal, J. C., Rivas, A. L., Chavanne, C., forthcoming. High-frequency frontal displacements south of San Jorge Gulf during a tidal cycle near spring and neap phases. Biological implications between tidal states. Oceanography.

Carreto, J. I., Carignan, M. O., Montoya, N. G., 2007. Ecología Del Fitoplancton En Los Sistemas Frontales del Mar Argentino. El Mar Argentino y sus recursos Pesqueros 5, 11–31.

Carreto, J. I., Lutz, V. A., Carignan, M. O., Cucchi-Colleoni, A. D., De Marco, S. G., 1995. Hydrography and chlorophyll a in a transect from the coast to the shelf-break in the Argentinian Sea. Continental Shelf Research 15 (2-3), 315–336.

Csirke, J., 1987. The Patagonian fishery resources and the off-shore fisheries in the South-West Atlantic. FAO Fisheries Technical Paper 287 (July), 75.

Cucchi-Colleoni, A. D., Carreto, J. I., 2001. Variación estacional de la biomasa fitoplanctónica en el Golfo San Jorge. Resultados de las Campañas de Investigación OB -01/00,OB-03/00 OB-07/00,OB-10/00 yOB-12/00. INIDEP, 1–30.

Dahll, E., Laake, M., Tjessem, K., Eberlein, K., B., B., 1983. Effects of Ekofisk crude oil on an enclosed planktonic ecosystem. Marine Ecology Progress Series 14, 81–91.

Dubinsky, E. a., Conrad, M. E., Chakraborty, R., Bill, M., Borglin, S. E., Hollibaugh, J. T., Mason, O. U., M. Piceno, Y., Reid, F. C., Stringfellow, W. T., Tom, L. M., Hazen, T. C., Andersen, G. L., 2013. Succession of hydrocarbon-degrading bacteria in the aftermath

of the deepwater horizon oil spill in the gulf of Mexico. Environmental Science and Technology 47 (19), 10860–10867.

Dunstan, W. M., Atkinson, L. P., Natoli, J., 1975. Stimulation and inhibition of phytoplankton growth by low molecular weight hydrocarbons. Marine Biology 31 (4), 305–310.

Fasham, M. J. R., Ducklow, H. W., McKelvie, S. M., aug 1990. A nitrogen-based model of plankton dynamics in the oceanic mixed layer. Journal of Marine Research 48 (3), 591–639.

Fernández, M., Carreto, J., Mora, J., Roux, A., 2005. Physico-chemical characterization of the benthic environment of the Golfo San Jorge, Argentina. Journal of the Marine Biological Association of the UK 85 (06), 1317–1328.

Fernandez, M., Roux, A., Fernndez, E., Cal, J., Marcos, A., Aldacur, H., 2003. Grain-size analysis of surficial sediments from Golfo San Jorge, Argentina. Journal of the Marine Biological Association of the UK 83 (6), 1193–1197.

Flores-Melo, X., Chavanne, C., Schloss, I. R., Almandoz, G. O., Latorre, M. P., Ferreyra, G. A., forthcoming. Phytoplankton ecology during a spring-neap tidal cycle in the southern tidal front of San Jorge Gulf, Patagonia. Oceanography.

Gin, K. Y., Huda, M. K., Lim, W. K., Tkalich, P., jul 2001. An oil spill-food chain interaction model for coastal waters. Marine pollution bulletin 42 (7), 590–7.

Glembocki, N. G., Williams, G. N., Góngora, M. E., Gagliardini, D. A., Orensanz, J. M. L., 2015. Synoptic oceanography of San Jorge Gulf (Argentina): A template for Patagonian red shrimp (Pleoticus muelleri) spatial dynamics. Journal of Sea Research 95, 22–35.

Glorioso, P., Simpson, J., feb 1994. Numerical modelling of the M2 tide on the northern Patagonian Shelf. Continental Shelf Research 14 (2-3), 267–278.

Glorioso, P. D., Flather, R. a., 1995. A barotropic model of the currents off SE South America. Journal of Geophysical Research 100 (95), 427–440.

Glorioso, P. D., Flather, R. a., 1997. The Patagonian Shelf tides. Progress in Oceanography 40 (1-4), 263–283.

González, J., Fernández, E., Figueiras, F., Varela, M., jun 2013. Subtle effects of the water soluble fraction of oil spills on natural phytoplankton assemblages enclosed in mesocosms. Estuarine, Coastal and Shelf Science 124, 13–23.

González, J., Figueiras, F. G., Aranguren-Gassis, M., Crespo, B. G., Fernández, E., Morán, X. A. G., Nieto-Cid, M., 2009. Effect of a simulated oil spill on natural assemblages of marine phytoplankton enclosed in microcosms. Estuarine, Coastal and Shelf Science 83 (3), 265–276.

Gordon, D. C., Prouse, N. J., 1973. The effects of three oils on marine phytoplankton photosynthesis. Marine Biology 22 (4), 329–333.

Grimes, D. J., Hazen, T. C., King, G. M., Prince, R. C., Carolina, N., Ward, C. H. H., Young, L., Maloy, S., 2011. Microbes & Oil Spills. Environmental Protection, 1–13.

Guerrero, R. A., Baldoni, A., Buenavides, H., 1999. Oceanographic conditions at the southern end of the argentine continental slope. INIDEP 5, 7–22.

Hamam, S. E. M., Hamoda, M. F., Shaban, H. I., Kilani, A. S., 1988. Crude oil dissolution in saline water. Water, Air, and Soil Pollution 37 (1-2), 55–64.

Harrison, W. G., Platt, T., 1986. Photosynthesis-irradiance relationships in polar and temperate phytoplankton populations. Polar Biology 5 (3), 153–164.

Hazen, T. C., Dubinsky, E. a., DeSantis, T. Z., Andersen, G. L., Piceno, Y. M., Singh, N., Jansson, J. K., Probst, A., Borglin, S. E., Fortney, J. L., Stringfellow, W. T., Bill, M., Conrad, M. E., Tom, L. M., Chavarria, K. L., Alusi, T. R., Lamendella, R., Joyner, D. C., Spier, C., Baelum, J., Auer, M., Zemla, M. L., Chakraborty, R., Sonnenthal, E. L., D'haeseleer, P., Holman, H.-Y. N., Osman, S., Lu, Z., Van Nostrand, J. D., Deng, Y., Zhou, J., Mason, O. U., 2010. Deep-sea oil plume enriches indigenous oil-degrading bacteria. Science (New York, N.Y.) 330 (6001), 204–208.

Head, I. M., Jones, D. M., Röling, W. F. M., 2006. Marine microorganisms make a meal of oil. Nature Reviews Microbiology 4 (3), 173–182.

Horowitz, A., Atlas, R. M., 1977. Continuous open flow-through system as a model for oil degradation in the arctic ocean. Applied and environmental microbiology 33 (3), 647–653.

Howarth, R. W., 1988. Nutrient Limitation of Net Primary Production in Marine Ecosystems. Annual Review of Ecology and Systematics 19 (1988), 89–110.

Hsiao, S. I., Kittle, D. W., Foy, M. G., 1978. Effects of crude oils and the oil dispersant corexit on primary production of arctic marine phytoplankton and seaweed. Environmental Pollution (1970) 15 (15), 209–221.

Hsiao, S. I. C., 1976. Biological Productivity of the Southern' Beaufort Sea: phytoplankton and seaweed studies. Fisheries and Marine Service Environment Canada 12, 99.

Johansson, S., Larsson, U., Boehm, P., 1980. The Tsesis oil spill impact on the pelagic ecosystem. Topics in Catalysis 11 (10), 284–293.

Kasai, Y., Kishira, H., Sasaki, T., Syutsubo, K., Watanabe, K., Harayama, S., mar 2002. Predominant growth of Alcanivorax strains in oil-contaminated and nutrient-supplemented sea water. Environmental microbiology 4 (3), 141–7.

King, G., Kostka, J., Hazen, T., Sobecky, P., 2015. Microbial Responses to the Deepwater Horizon Oil Spill: From Coastal Wetlands to the Deep Sea. Annual Review of Marine Science 7 (1), 377–401.

Krepper, C., Rivas, A. L., 1979. Análisis de las características oceanográfica de la zona austral de la Plataforma Continental Argentina y aguas adyacentes. Acta Oceanográfica Argentina 2 (2), 55–82.

Latorre, M. P., Schloss, I. R., Almandoz, G. O., Lemarchand, K., Flores-Melo, X., Massé-Baulne, V., Ferreyra, G. A., forthcoming. Mixing processes at the pycnocline and vertical nutrients supply: Consequences for the microbial community in the San Jorge Gulf (Argentina). Oceanography.

Lima, I. D., Olson, D. B., Doney, S. C., 2002. Intrinsic dynamics and stability properties of size-structured pelagic ecosystem models. J. Plankton Res. 24 (6), 533–556.

Louge, E. B., Reta, R., Santos, B. A., Hernandez, D. R., 2004. Variaciones interanuales (1995-2000) de la temperatura y la salinidad registradas en los meses de enero en el Golfo San Jorge y aguas adyacentes (43S-47S). Revista de Investigacion y Desarrollo Pesquero 16 (Contribucion INIDEP 1275), 27–42.

Ministerio de Energía y Minería, 2016. Producción de petróleo en Argentina desde 1950. Tech. rep., Subsecretaría de Escenarios y Evaluación de Proyectos - Secretaría de Planeamiento Energético Estratégico.
URL https://datos.minem.gob.ar/dataset

Mulkins-Phillips, G. J., Stewart, J., 1974. Distribution of hydrocarbon-utilizing bacteria in Northwestern Atlantic waters and coastal sediments. Canadian journal of microbiology 20 (7), 955–956.

Musser, B. J., Kilpatrick, P. K., Carolina, N., 1999. Molecular characterization of wax isolated from a variety of crude oils. Fuel and Energy Abstracts 40 (1), 18.

Nayar, S., Goh, B. P. L., Chou, L. M., apr 2005. Environmental impacts of diesel fuel on bacteria and phytoplankton in a tropical estuary assessed using in situ mesocosms. Ecotoxicology (London, England) 14 (3), 397–412.

Palma, E. D., Matano, R. P., 2012. A numerical study of the Magellan Plume. Journal of Geophysical Research: Oceans 117 (5), 1–16.

Palma, E. D., Matano, R. P., Piola, A. R., 2004. A numerical study of the Southwestern Atlantic Shelf circulation: Barotropic response to tidal and wind forcing. Journal of Geophysical Research 109 (C8), C08014.

Petroleum HPV Testing Group, 2011. Crude Oil Category Assessment Document. Tech. rep., The American Petroleum Institute.

Piola, A. R., Rivas, A. L., 1997. Corrientes en la Plataforma Continental. El Mar Argentino y sus recursos Pesqueros 1, 119–132.

Potters, G., 2013. Marine Pollution, 1st Edition. Bookboon.

Prince, R. C., Lessard, R. R., Clark, J. R., 2003. Bioremediation of marine oil spills. Trends in biotechnology 58 (4), 463–468.

Reddy, C. M., Arey, J. S., Seewald, J. S., Sylva, S. P., Lemkau, K. L., Nelson, R. K., Carmichael, C. a., McIntyre, C. P., Fenwick, J., Ventura, G. T., Van Mooy, B. a. S., Camilli, R., dec 2012. Composition and fate of gas and oil released to the water column during the Deepwater Horizon oil spill. Proceedings of the National Academy of Sciences of the United States of America 109 (50), 20229–34.

Reed, M., Johansen, Ø., Brandvik, P. J., Daling, P., Lewis, A., Fiocco, R., MacKay, D., Prentki, R., 1999. Oil spill modeling towards the close of the 20th century: Overview of the state of the art. Spill Science and Technology Bulletin 5 (1), 3–16.

Rivas, A. L., Dogliotti, A. I., Gagliardini, D. a., apr 2006. Seasonal variability in satellite-measured surface chlorophyll in the Patagonian Shelf. Continental Shelf Research 26 (6), 703–720.

Sargian, P., Mas, S., Pelletier, É., Demers, S., jan 2007. Multiple stressors on an Antarctic microplankton assemblage: water soluble crude oil and enhanced UVBR level at Ushuaia (Argentina). Polar Biology 30 (7), 829–841.

Shiller, A. M., Joung, D., 2012. Nutrient depletion as a proxy for microbial growth in Deepwater Horizon subsurface oil/gas plumes. Environmental Research Letters 7 (4), 045301.

Simpson, J., Hunter, J., Bowden, K., 1974. Fronts in the Irish Sea. Nature 250 (5465), 404–406.

Siron, R., Pelletier, E., Roy, S., aug 1996. Effects of dispersed and adsorbed crude oil on microalgal and bacterial communities of cold seawater. Ecotoxicology (London, England) 5 (4), 229–51.

Syutsubo, K., Kishira, H., Harayama, S., 2001. Development of specific oligonucleotide probes for the identification and in situ detection of hydrocarbon-degrading Alcanivorax strains. Environmental Microbiology 3 (6), 371–379.

Teal, J. M., Howarth, R. W., 1984. Oil Spill Studies: A Review of Ecological Effects. Environmental Management 8 (1), 27–44.

Tremblay, J.-É., Michel, C., Hobson, K. A., Gosselin, M., Price, N. M., 2006. Bloom dynamics in early opening waters of the Arctic Ocean. Limnology and Oceanography 51 (2), 900–912.

Valentine, D. L., Mezic, I., Macesic, S., Crnjaric-Zic, N., Ivic, S., Hogan, P. J., Fonoberov, V. A., Loire, S., 2012. Dynamic autoinoculation and the microbial ecology of a deep water hydrocarbon irruption. Proceedings of the National Academy of Sciences 109 (50), 20286–20291.

Yakimov, M. M., Timmis, K. N., Golyshin, P. N., jun 2007. Obligate oil-degrading marine bacteria. Current opinion in biotechnology 18 (3), 257–66.